ESD-TR-67-266
ESTI FILE COPY

ESD-TR-67-266

ESD RECORD COPY
RETURN TO
SCIENTIFIC & TECHNICAL INFORMATION DIVISION
ESD, BEDFORD, MASS.

ESD ACCESSION LIST
ESTI Call No. AL 57398
Copy No. 1 of 1 cys.

2

Solid State Research

1967

Prepared under Electronic Systems Division Contract AF 19(628)-5167 by

Lincoln Laboratory

MASSACHUSETTS INSTITUTE OF TECHNOLOGY

Lexington, Massachusetts

AD0656548

The work reported in this document was performed at Lincoln Laboratory, a center for research operated by Massachusetts Institute of Technology, with the support of the U.S. Air Force under Contract AF 19(628)-5167.

This report may be reproduced to satisfy needs of U.S. Government agencies.

Distribution of this document is unlimited.

Non-Lincoln Recipients

PLEASE DO NOT RETURN

Permission is given to destroy this document when it is no longer needed.

2

Solid State Research

1967

Issued 5 July 1967

Lincoln Laboratory

MASSACHUSETTS INSTITUTE OF TECHNOLOGY

Lexington, Massachusetts

ABSTRACT

This report covers in detail the solid state research work at Lincoln Laboratory for the period 1 February through 30 April 1967. The topics covered are Solid State Device Research, Optical Techniques and Devices, Materials Research, and Physics of Solids.

Accepted for the Air Force
Franklin C. Hudson
Chief, Lincoln Laboratory Office

INTRODUCTION

1. SOLID STATE DEVICE RESEARCH

Single crystals of $Pb_{1-y}Sn_ySe$ have been grown by the Bridgman technique with compositions up to y = 0.3. The as-grown material exhibits a very high degree of Pb-Sn ratio homogeneity but is consistently heavily p-type with high carrier densities. Carrier concentrations and 77°K Hall mobilities of 9×10^{16} cm^{-3} and 25,000 cm^2/V sec in p-type material, and of 1.5×10^{17} cm^{-3} and 42,000 cm^2/V sec in n-type material, have been obtained by annealing the material in a two-zone furnace.

The interdiffusion parameters of Pb and Se in PbSe have been studied by introducing controlled deviations from the stoichiometric concentration. Excess Se was diffused into Pb-rich n-type material and excess Pb was diffused into Se-rich p-type material, forming in each case a p-n junction. The diffusion constants were obtained by plotting the junction depth as a function of time.

$Pb_{1-y}Sn_ySe$ lasers and photovoltaic detectors have been fabricated over a wide composition range. Laser emission has now been observed out to 18.9 μ and photovoltaic response to 22 μ at 12°K. Close agreement is observed between the emission wavelength and the cutoff wavelength of the photovoltaic response in lasers and detectors fabricated from the same material. Results show that the energy gap of $Pb_{1-y}Sn_ySe$ varies with Sn content in much the same manner as that of $Pb_{1-x}Sn_xTe$.

Efficient photovoltaic detectors of infrared radiation at wavelengths up to 11 μ which operate at 77°K have been fabricated from annealed Bridgman-grown $Pb_{1-y}Sn_ySe$ single crystals. Responsivities of 3 V/W at 77°K, and internal quantum efficiencies of about 20 percent, have been obtained. The detector noise is less than the noise of the measuring system yielding an upper noise limit of 10^{-10} V sec. This corresponds to a minimum D* of 3×10^9 cm/W $sec^{1/2}$ near the peak at 11 μ. The detector risetime at 77°K is 20 nsec which can be accounted for by the RC time constant of the device.

A method has been proposed by which infrared radiation is efficiently converted directly to visible radiation by a single solid state device. The device consists of a capacitor-photodetector-photoemitter sandwich in which infrared radiation is incident on one face and the visible radiation is emitted from the opposite face. The low level current produced by the infrared detector is integrated and stored by the capacitor and then delivered to the light emitter in short high current pulses. The feasibility of such a pulsed device has been demonstrated using an indium antimonide diode detector and a gallium arsenide-phosphide diode emitter to convert infrared radiation of wavelengths up to 5.3 μ into visible radiation between 0.6 and 0.7 μ with a quantum efficiency of 10^{-4}.

Electroluminescence has been observed at 4.2° and 77°K from CdS vapor-grown single crystal platelets with indium contacts bonded to opposite faces of the 10- to 20-μ thick samples.

Current densities as high as 2×10^4 A cm^{-2} under pulsed conditions and 100 A cm^{-2} DC have been obtained. At low temperatures, luminescence appears at about 10 A cm^{-2} DC with light intensity increasing rapidly with current. External quantum efficiencies between 10^{-6} and 10^{-5} were obtained at 10^3 A cm^{-2}.

We have obtained laser emission from ZnTe excited by an electron beam with up to 90 W of peak output power at 5280 Å and 8-percent overall power efficiency at liquid helium temperature, and up to 25 W at 5310 Å and 2-percent overall power efficiency at 77°K. The lowest threshold observed was 48 keV, which is high compared with the other II-VI compounds.

II. OPTICAL TECHNIQUES AND DEVICES

A CW Doppler radar has been constructed using a 5-W CO_2 laser and a helium-cooled Cu-doped Ge heterodyne detector. Moving vehicles have been detected out to ranges of 2 miles.

A sealed-off 5-W CO_2 laser tube has been operated for more than 700 hours by reclaiming the CO_2 gas from the cathode region. The CO_2 adsorption at the nickel cathode was reversible, and this gas was again replaced in the tube fill by heating the cathode region to 300°C.

Narrow-band operation of a $Pb_{1-x}Sn_xSe$ photovoltaic detector at 77°K has yielded heterodyne detection sensitivities close to the theoretical limit.

Faraday rotation in indium antimonide is being used to construct an isolator at 10.6-μm wavelength.

III. MATERIALS RESEARCH

Single crystals of $MnBr_2$ have been grown from the melt and from the vapor phase by a method in which helium was used as a carrier gas to transport $MnBr_2$ vapor produced by the reaction between Br_2 vapor and Mn powder at 850°C. A large-grained ingot of EuO was prepared in a sealed molybdenum crucible by solidification of a nonstoichiometric melt heated to 2000°C and slowly cooled.

Isothermal measurements of resistivity as a function of time for S-doped GaSb have shown that the transfer of electrons from the conduction band to the sulfur donor levels is characterized by two time constants, both of which vary exponentially with reciprocal temperature. The slower constant increases from 5 min. at 90°K to 1300 min. at 77°K, and the faster constant increases from 1.6 to 230 min. over the same temperature range.

Data on the resistivity of Ag_2Te as a function of temperature and hydrostatic pressure have been used to construct a pressure-temperature diagram for this compound. The structure of Ag_2Te-III, which is the stable phase at room temperature for pressures above 25 kbars, was found to be tetragonal on the basis of x-ray diffraction results obtained with a new high-pressure camera.

The effect of high pressure on the properties of titanium monoxide (TiO_x), which has the rocksalt structure, has been studied by annealing samples with x between 0.87 and 1.06 at about 50 kbars and 1100° to 1300°C for 1 to 3 hours. This treatment reduced the concentration of vacancies from 14 – 15 to 11 – 13 percent of the total number of lattice sites, and increased the superconducting transition temperature from less than 1.2°K to between 1.3° and 1.8°K.

Measurements with a vibrating coil magnetometer have shown that the Curie temperature of ferromagnetic $SrRuO_3$, which is 164°K at atmospheric pressure, decreases linearly with increasing hydrostatic pressure at the rate of 0.63°/kbar. This decrease supports the hypothesis that the magnetic properties of this material are primarily due to band effects rather than to localized moments.

An electron density difference map for $PbRuO_3$ has been obtained by computer calculation from integrated x-ray intensity data. This map confirms the existence of a trap-mediated Pb-Pb bond in $PbRuO_3$, as proposed previously on the basis of structure refinement calculations.

An analysis has been made of the factors influencing the Néel temperature in magnetic materials with perovskite and related structures. It was shown that the theoretical expression for the variation of Néel temperature with lattice parameter cannot be adequately tested if the lattice parameter is changed by chemical substitution rather than by applying pressure.

IV. PHYSICS OF SOLIDS

In extending the magnetoelectroreflection studies, a mechanically integrated thin film package has been developed. This dry package has eliminated the temperature and wavelength restrictions which have limited the liquid electrolyte technique, thereby making the method competitive with piezoreflectance.

The anomalous exciton peaks previously reported for InSb have not been observed in germanium. This result, taken in conjunction with calculations by Bell and Rogers, suggests that the anomalies arise from the lack of inversion symmetry of InSb.

A magneto-optical investigation is being undertaken to determine energy band changes in the transition from semimetal to semiconductor as bismuth is alloyed with antimony. To date, sharp magnetoreflection oscillations have been observed in the alloy $Bi_{0.97}Sb_{0.03}$.

The current modulated reflectance data of gold has been analyzed. Qualitative agreement with the observed structure was obtained.

Recent experimental investigations of the magnetic energy levels of donor impurities in InSb have prompted a variational calculation of the impurity ground state and the lowest lying $M = \pm 1$ excited states. Comparison of the results with experiment suggests tentatively a central cell correction which increases with magnetic field.

Introduction

Work on the phonon dispersion relations for silicon and germanium is continuing. By incorporating the shell model within the Fourier expansion technique, a more rapid convergence of the series is obtained; for silicon, calculations using up to and including fourth-nearest-neighbor terms for the ion cores, and the lowest nonvanishing terms for the core shell interaction, give reasonable agreement with the experimental neutron diffraction data.

In order to explain the transport anomalies in Ti_2O_3, a two-band model has been proposed. By allowing the energy band structure to change continuously in the temperature region of sharp resistivity change (540°K), a resistivity is calculated which agrees with the experiments in all important respects, unlike the magnetic phase transition theory which is inconsistent with the magnetoresistance data.

The Landau transport equation of a Fermi liquid in the presence of dilute random impurities has been attacked by the temperature technique of Luttinger and Ward. Although the calculation has been carried out only in the limit of zero temperature, it is felt that the first temperature corrections may be obtained from this method.

In the continuing study of distant neighbor magnetic interactions in spinels with nonmagnetic A-sites, preliminary neutron diffraction measurements in $ZnCr_2S_4$ indicate a rather complicated spiral pattern at very low temperatures. A thorough study of the magnetic behavior of this material is planned in collaboration with Brookhaven National Laboratory.

Antiferromagnetic resonance in the frequency range 35 to 70 GHz has been observed in single crystals of MnI_2 at liquid helium temperatures where the Mn^{2+} spins order in a flat spiral configuration. In addition to the main resonance, several weaker ones were observed; a theoretical analysis is being attempted.

High temperature expansions of the internal energy, entropy and specific heat for the classical Heisenberg model have been carried out. The first ten coefficients have been numerically evaluated for various two- and three-dimensional lattices. This expansion technique has also been used to obtain expressions for the zero-field reduced susceptibilities of the Ising and Heisenberg models and to show the similarity between them.

Electronic Raman scattering has now been obtained from phosphorous donors and boron acceptors in silicon. Phonon Raman scattering involving the creation of one virtual zone-center optical phonon with subsequent decay through the anharmonic interaction into two acoustic phonons has also been observed.

The ultraviolet-pumping model for interstellar 18-cm OH emission and anomalous absorption has been extended to include effects of thermal electron collisions, overlapping pump absorption lines, and selective far infrared absorption. Analyses have been made of the possibility of maser action in SH, of unusual gain frequency profiles, and of stability of pure circularly polarized emission.

Investigation is continuing of the mode structure in a resonant Raman oscillator consisting of a quartz sample cavity with plane, parallel end faces. The spacing of the modes, which

is consistently 20 percent closer than expected from the cavity lengths, is likely to be caused by quartz resonator mode pulling.

A technique has been developed for producing high-power pulses of coherent light with frequency continuously tunable over a 1000-Å range. Although so far the method has been used to generate visible light, in principle it is applicable for a tunable far infrared source.

High power mode locked output has been obtained in a rotating prism Q-switched ruby laser without the use of separate cavity modulators. The number of modes involved is small and the deduced peak power is 50 MW.

A cyanide laser, which operates at 337μ, has been constructed. It will be used for far infrared spectroscopic investigations.

CONTENTS

Abstract iii
Introduction v
Organization xii
Reports by Authors Engaged in Solid State Research xiii

I. SOLID STATE RESEARCH 1

A. Crystal Growth, Composition Control and Junction Formation in the Lead-Tin Chalcogenides 1

B. Diffusion Studies in Lead Salts 4

C. Bandgap Determination from Laser Emission and Photovoltaic Response Measurements in $Pb_{1-y}Sn_ySe$ Diodes 6

D. Properties of $Pb_{1-y}Sn_ySe$ Infrared Detectors 7

E. InSb-GaAsP Infrared to Visible Light Converter 9

F. Electroluminescence in CdS 11

G. Laser Emission from Electron-Beam-Excited ZnTe 11

II. OPTICAL TECHNIQUES AND DEVICES 15

A. CO_2 Laser Radar System 15

B. Sealed CO_2 Laser Tube with Greater than a 700-Hour Life 16

C. Photovoltaic Heterodyne Detection in $Pb_{1-x}Sn_xSe$ 17

D. Faraday Isolator 18

III. MATERIALS RESEARCH 19

A. Crystal Growth 19

B. Kinetics of Electron Transfer Between Conduction Band and Sulfur Donors in GaSb 19

C. Polymorphism in Ag_2Te at High Pressures and Temperatures 21

D. Effect of High Pressure on Oxides with Defect-Rocksalt Structures 24

E. Effect of Hydrostatic Pressure on the Curie Point of $SrRuO_3$ 25

F. Election Density Difference Map as Further Evidence for Trap-Mediated Pb-Pb Bond in $PbRuO_3$ 26

G. Néel Temperatures in Perovskite and Related Structures 27

IV. PHYSICS OF SOLIDS 31

A. Electronic Band Structure 31

B. Transport Phenomena 35

C. Magnetism 37

D. Scattering Experiments with Lasers 45

ORGANIZATION

SOLID STATE DIVISION

A. L. McWhorter, *Head*
P. E. Tannenwald, *Associate Head*
M. J. Hudson, *Assistant*
E. P. Warekois

SOLID STATE THEORY

H. J. Zeiger, *Leader*
M. M. Litvak, *Assistant Leader*

Argyres, P. N.
Chinn, S. R.†
Dresselhaus, G. F.
Hanus, J.
Kaplan, T. A.
Kelley, P. L.
Kleiner, W. H.
Larsen, D. M.
Melanson, G. S., Jr.
Palm, B. J.*
Stanley, H. E.
Trent, P. H.
Van Zandt, L. L.

OPTICS AND INFRARED

R. H. Kingston, *Leader*
R. J. Keyes, *Assistant Leader*

Bates, D. H.
Bostick, H. A.
Carbone, R. J.
Dennis, J. H.
Freed, C.
Longaker, P. R.
McPhie, J. M.
Quist, T. M.
Ross, A. H. M.
Sullivan, F. M.
Teich, M. C.
Zimmerman, M. D.

ELECTRONIC MATERIALS

J. B. Goodenough, *Leader*
J. M. Honig, *Associate Leader*
A. J. Strauss, *Assistant Leader*

Anderson, C. H., Jr.
Andrews, H. I.†
Arnott, R. J.
Banus, M. D.
Batson, D.
Brebrick, R. F., Jr.
Button, M. J.
Delaney, E. J.
England, R. E.
Fahey, R. E.
Ferretti, A.
Finn, M. C.
Hilsenrath, S.
Iseler, G. W.
Kafalas, J. A.
LaFleur, W. J.
Lavine, M. C.*
Longo, J. M.
Mastromattei, E. L.
O'Connor, J. R.
Owens, E. B.
Plonko, M. C.
Pollard, E. R.†
Raccah, P. M.
Reed, T. B.
Roddy, J. T.
Searles, I. H.
Sohn, J. B.
Soracco, D. J.
Steininger, J. A.

SOLID STATE PHYSICS

J. G. Mavroides, *Leader*
G. B. Wright, *Assistant Leader*

Burke, J. W.
Carman, R. L.*
Dickey, D. H.
Dresselhaus, M. S.
Dwight, K., Jr.
Feinleib, J.
Feldman, B.
Fulton, M. J.
Groves, S. H.
Johnson, E. J.
Kernan, W. C.
Kolesar, D. F.
Krag, W. E.
Melngailis, J.
Menyuk, N.
Murphy, H. C.
Nill, K. W.
Parker, C. D.
Perry, F. H.
Scouler, W. J.
Stickler, J. J.†
Strahm, N. D.†
Thaxter, J. B.
Tichovolsky, E. J.†
Weber, R.

APPLIED PHYSICS

J. O. Dimmock, *Leader*
T. C. Harman, *Assistant Leader*
I. Melngailis, *Assistant Leader*

Butler, J. F.
Calawa, A. R.
Carter, F. B.
Caswell, F. H.
Clough, T. F.
Donaldson, P. L.
Donnelly, J. P.
Finne, P.
Foyt, A. G.
Hinkley, E. D.
Hurwitz, C. E.
Lindley, W. T.
Mooradian, A.
Oliver, M. R.†
Paladino, A. E.
Phelan, R. J., Jr.
Ward, J. H. R., III
Wolfe, C. M.
Youtz, P.

---

* Part Time
† Research Assistant

REPORTS BY AUTHORS ENGAGED IN SOLID STATE RESEARCH

15 February through 15 May 1967

PUBLISHED REPORTS

Journal Articles*

JA No.			
2581	Magnetic Quantum Effects	P.N. Argyres L.M. Roth†	Semiconductors and Semimetals, Vol. 1, Physics of III-V Compounds, edited by R.K. Willardson and A.C. Beer (Academic Press, New York, 1966)
2747	Space-Time Symmetry Restrictions on Transport Coefficients. II. Two Theories Compared	W.H. Kleiner	Phys. Rev. 153, 726 (1967)
2796	Comparison of the Theoretical O^{--} Form Factors with Experiment	P.M. Raccah R.J. Arnott	Phys. Rev. 153, 1028 (1967) DDC 651719
2837	Low Temperature Crystallographic and Magnetic Study of $LaCoO_3$	N. Menyuk K. Dwight P.M. Raccah	J. Phys. Chem. Solids 28, 549 (1967)
2872	A First-Order Localized-Electron ⇄ Collective-Electron Transition	P.M. Raccah J.B. Goodenough	Phys. Rev. 155, 932 (1967)
2873	Hartree-Fock Theory: Slater Determinants of Minimum Energy	T.A. Kaplan W. H. Kleiner	Phys. Rev. 156, 1 (1967)
2875	Virial Theorem for the Homogeneous Electron Gas	P.N. Argyres	Phys. Rev. 154, 410 (1967)
2878	Low Temperature Absolute Reflection Measurements of Small Samples	J. Feinleib B. Feldman	Rev. Sci. Instr. 38, 32 (1967)
2887	Spark-Source Mass Spectroscopy	E.B. Owens	Appl. Spectroscopy 21, 1 (1967)
2890	Interband Magnetooptical Studies of Semiconductors and Semimetals	B. Lax† J.G. Mavroides	Appl. Optics 6, 647 (1967)

* Reprints available.

† Author not at Lincoln Laboratory.

Reports

JA No.			
2903	Excitation Spectra of Group III Impurities in Germanium Under Uniaxial Stress	D.H. Dickey J.O. Dimmock	J. Phys. Chem. Solids 28, 529 (1967)
2918	Semiconductor-to-Metal Transitions in Transition-Metal Compounds	D. Adler* J. Feinleib H. Brooks* W. Paul*	Phys. Rev. 155, 851 (1967)
2920	Semiconductor-to-Metal Transition in V_2O_3	J. Feinleib W. Paul*	Phys. Rev. 155, 841 (1967)
2921	On the Thermodynamic Properties of Several Solid Phases of the Compound InSb	A.K. Jena* M.B. Bever* M.D. Banus	Trans. Met. Soc. 239, 725 (1967)
2923	Diode Lasers of $Pb_{1-y}Sn_ySe$ and $Pb_{1-x}Sn_xTe$	J.F. Butler A.R. Calawa T.C. Harman	Appl. Phys. Letters 9, 427 (1966)
2927	Polaron Effects in the Cyclotron-Resonance Absorption of InSb	D.H. Dickey E.J. Johnson D.M. Larsen	Phys. Rev. Letters 18, 599 (1967)
2928	Temperature-Modulated Reflectance of Gold from 2 to 10 eV	W.J. Scouler	Phys. Rev. Letters 18, 445 (1967)
2932	High Power and Efficiency in CdS Electron Beam Pumped Lasers	C.E. Hurwitz	Appl. Phys. Letters 9, 420 (1966)
2946	InSb MOS Infrared Detector	R.J. Phelan, Jr. J.O. Dimmock	Appl. Phys. Letters 10, 55 (1967)
2948	The Electrical Properties and Band Structure of Doped $LaInO_3$	D.B. Rogers* J.M. Honig J.B. Goodenough	Materials Res. Bull. 2, 223 (1967)
2965	Identification of the Fundamental Vibrational Modes of Trigonal, α-Monoclinic and Amorphous Selenium	G. Lucovsky* A. Mooradian W. Taylor* G.B. Wright R.C. Keezer*	Solid State Commun. 5, 113 (1967)
2988	Raman Scattering from Donor and Acceptor Impurities in Silicon	G.B. Wright A. Mooradian	Phys. Rev. Letters 18, 608 (1967)
MS No.			
1422	Theory of the Method of Kinetic Equations for Quantum Systems	P.N. Argyres	Lectures in Theoretical Physics, Vol. 8A (University of Colorado Press, 1966)
1702	Optical and Laser Properties of Nd^{+3}- and Eu^{+3}-Doped YVO_4	J.R. O'Connor	Trans. Met. Soc. 239, 362 (1967)

* Author not at Lincoln Laboratory.

MS No.			
1746	Dependence of Critical Properties of Heisenberg Magnets upon Spin and Lattice	H.E. Stanley T.A. Kaplan	J. Appl. Phys. 38, 977 (1967)
1747	On the Possible Phase Transition for Two-Dimensional Heisenberg Models	H.E. Stanley T.A. Kaplan	J. Appl. Phys. 38, 975 (1967)
1791	Spontaneous Band Magnetism	J.B. Goodenough	J. Appl. Phys. 38, 1054 (1967)
1814-II	Characterization of d Electrons in Solids by Structure. II. Spontaneous Crystallographic Distortions	J.B. Goodenough	Materials Res. Bull. 2, 165 (1967)
1815	Experimental Techniques with General Applicability for the Study of Magnetic Phenomena	K. Dwight	J. Appl. Phys. 38, 1505 (1967)

UNPUBLISHED REPORTS

Journal Articles

JA No.			
2850	High-Temperature Expansions for the Classical Heisenberg Model. I. Spin Correlation Function	H.E. Stanley	Accepted by Phys. Rev.
2907	High-Temperature Expansions for the Classical Heisenberg Model. II. Zero-Field Susceptibility	H.E. Stanley	Accepted by Phys. Rev.
2939	Fourier Expansion for the Electronic Energy Bands in Silicon and Germanium	G.F. Dresselhaus M.S. Dresselhaus	Accepted by Phys. Rev.
2964	Temperature Dependence, Orientation Correlation and Molecular Fields in Second Harmonic Light Scattering from Liquids and Gases	D.L. Weinberg	Accepted by J. Chem. Phys.
2973	The Crystal Structure of Neodymium Monotellurooxide-Nd_2O_2Te	P.M. Raccah J.M. Longo H.A. Eick*	Accepted by Inorg. Chem.
2975	Report on the Seventh International Conference on the Physics of Semiconductors	B. Lax* J.G. Mavroides	Accepted by Phys. Today
2977	Interband Magnetoreflection and Band Structure of HgTe	S.H. Groves R.N. Brown* C.R. Pidgeon*	Accepted by Phys. Rev.
2978	Magnetoplasma Cyclotron Absorption in PbSe	S. Bermon	Accepted by Phys. Rev.

* Author not at Lincoln Laboratory.

Reports

JA No.			
2989	A Thermodynamic Investigation of the Compounds In_3SbTe_2, InSb and InTe	A. K. Jena* M. B. Bever* M. D. Banus	Accepted by Trans. Met. Soc. AIME
2993	Magnetic and Structural Study of the Spinel $MnYb_2S_4$	M. J. Longo P. M. Raccah	Accepted by Materials Res. Bull.
2994	Stability Measurements of CO_2-N_2-He Lasers at 10.6 μm Wavelength	C. Freed	Accepted by IEEE J. Quant. Electron.
2998	Hall Coefficient and Transverse Magnetoresistance in HgTe at 4.2°K and 77°K	T. C. Harman J. M. Honig P. Trent	Accepted by J. Phys. Chem. Solids
3018	Growth of Single Ti_2O_3 Crystals from the Melt	T. B. Reed R. E. Fahey J. M. Honig	Accepted by Materials Res. Bull.
3023	Laser Emission from Electron Beam Excited ZnTe	C. E. Hurwitz	Accepted by IEEE J. Quant. Electron.

Meeting Speeches †

MS No.			
1629B	Spontaneous Band Ferromagnetism in Metallic Oxides	J. B. Goodenough	Materials Research Unit Seminar, McMaster University, Ontario, Canada, 20 March 1967
1629C	Relation Between Structural and Magnetic Properties of Transition-Metal Compounds	J. B. Goodenough	Solid State Chemistry Conference, Brown University, 3 – 5 April 1967
1836	Effect of High Pressures on the Structures and Properties of Some Solids	M. D. Banus	Solid State Chemistry Conference, Brown University, 3 – 5 April 1967
1719E	Interstellar OH Maser Emission	A. L. McWhorter	Seminar, University of Colorado, 17 March 1967
1787B	Spin Waves in Paramagnetic Fermi Gases	L. L. Van Zandt	Seminar, Wayne State University, Detroit, Michigan, 16 February 1967
1793A	Polaron Self-Energy Effects in InSb	E. J. Johnson	Seminar, Purdue University, 7 March 1967
1830B	Metallic Properties of Certain Metal Oxides	J. M. Honig	Colloquium, Brandeis University, 7 March 1967

* Author not at Lincoln Laboratory.

† Titles of Meeting Speeches are listed for information only. No copies are available for distribution.

MS No.			
1846A, B	An Effective Hamiltonian for the Optical Properties of Si and Ge	G. F. Dresselhaus	Seminar, New York University, 24 February 1967; Colloquim, University of Illinois, 17 March 1967
1848	Kinetics of Electron Transfer Between Conduction Band and Sulfur Donors in GaSb	G. W. Iseler A. J. Strauss	American Physical Society, Chicago, 27 – 30 March 1967
1860	Fourier Expansion of the Phonon Dispersion Relations for Silicon and Germanium	G. F. Dresselhaus	
1861	Magnetooptical Evidence for the Existence of a Complex Band Edge at the Energy Gap of the Layer Compound GaSe	J. Halpern J. L. Brebner* E. Mooser*	
1866	Current Modulated Reflectance of Nickel from 0.1 to 10eV	W. J. Scouler J. Feinleib J. Hanus	
1867	Observation of Exciton Fine Structure in the Interband Magneto-Atsorption of InSb	E. J. Johnson	
1868	Magnetoelectroreflectance at 1.5°K	C. R. Pidgeon* J. Feinleib S. H. Groves R. J. Phelan, Jr.	
1869	NMR in the Ferromagnetic Semiconductor $CdCr_2Se_4$	M. Rubinstein* G. H. Stauss* J. Feinleib A. Wold*	
1873	Critical Behavior of the Zero-Field Susceptibility for Heisenberg Models	H. E. Stanley	
1874	Negative Magnetoresistance Effects in Ti_2O_3	J. M. Honig L. L. Van Zandt J. B. Sohn T. B. Reed	
1875	Symmetry of the Ground Level of a Hamiltonian	W. H. Kleiner T. A. Kaplan	
1876	High Efficiency Infrared Photovoltaic Effect in Metal-Oxide-Semiconductor Structures	R. J. Phelan, Jr. J. O. Dimmock	
1877	Observations on the Existence of a Phase Transition in Two-Dimensional Heisenberg Models	T. A. Kaplan H. E. Stanley	

* Author not at Lincoln Laboratory.

Reports

MS No.			
1878	Landau Damping of Magneto-plasma Waves for General Closed Fermi Surfaces	A. L. McWhorter J. N. Walpole*	American Physical Society, Chicago, 27 – 30 March 1967
1880	Laser Action and Photovoltaic Effect in $Pb_{1-y}Sn_ySe$ Diodes	J. F. Butler A. R. Calawa I. Melngailis T. C. Harman J. O. Dimmock	
1882	Raman Scattering from Plasmons and Phonons	A. Mooradian	
1891B	Inversion of Conduction and Valence Bands in $Pb_{1-x}Sn_xSe$ Alloys	A. J. Strauss	
1924	Microwave Magnetoacoustic Effects in Indium Antimonide	K. W. Nill	
1931	Optical Modulation in Semi-conductors and Metals	J. Feinleib	
1850	Recent Developments in Mass Spectroscopy	E. B. Owens	Society of Applied Spectroscopy, Newton, Massachusetts, 10 January 1967
1882B	Raman Scattering in Semiconductors	A. Mooradian	Seminar, Purdue University, 7 April 1967
1882C	Raman Scattering from Plasmons and Phonons	G. B. Wright	Seminar, M. I. T., 11 April 1967
1891	Physical Properties and Band Structure of $Pb_{1-x}Sn_xSe$ Alloys	A. J. Strauss	Colloquium, Naval Ordnance Laboratory, Silver Spring, Maryland, 21 February 1967
1899	Properties of $Pb_{1-x}Sn_xTe$ and $Pb_{1-x}Sn_xSe$ Infrared Detectors	I. Melngailis	IRIS Infrared Detector Specialty Group, Wright-Patterson Air Force Base, 6 – 7 March 1967
1907	Physical Properties and Band Structure of $Pb_{1-x}Sn_xTe$ and $Pb_{1-x}Sn_xSe$ Alloys	A. J. Strauss T. C. Harman	
1908	Infrared Heterodyne Detection of CO_2 Laser Radiation in Ge:Cu and in $Pb_xSn_{1-x}Te$	M. C. Teich	
1903	Light-by-Light Scattering and Pulse Self-Steepening	P. L. Kelley	Seminar, Ford Motor Scientific Research Laboratory, Dearborn, Michigan, 13 February 1967

* Author not at Lincoln Laboratory.

MS No.			
1904	High-Temperature Expansion of the Spin Correlation Function for Heisenberg Models	H.E. Stanley	Seminar, Bell Telephone Laboratories, Murray Hill, New Jersey, 16 February 1967
1915	The Heisenberg Model of Magnetism	H.E. Stanley	Colloquium, Temple University, 6 March 1967
1919	Band Structure and Applications of $Pb_{1-x}Sn_xTe$ and $Pb_{1-y}Sn_ySe$	I. Melngailis	Seminar, Colorado State University, 2 March 1967
1931B, C	Optical Modulation in Semiconductors and Metals	J. Feinleib	Seminar, Harvard University, 26 April 1967; Seminar, Ford Motor Scientific Research Laboratories, Dearborn, Michigan, 8 May 1967
1952A	Observation of Magneto-Elastic Coupling by Spin Wave Resonance	R. Weber	Seminar, Case Institute, Cleveland, Ohio, 9 May 1967
1964	On High-Temperature Expansions for the Heisenberg Model	H.E. Stanley	17th Statistical Mechanics Meeting, Yeshiva University, New York, 6 April 1967
1968	Negative Magnetoresistance Effects in Ti_2O_3	L.L. Van Zandt	Seminar, Purdue University, 25 April 1967
1975	A Carbon Dioxide Laser Radar System	H.A. Bostick	3rd DoD Conference on Laser Technology, Pensacola, Florida, 18 – 20 April 1967
1977	Polarons in Indium Antimonide	D.M. Larsen	Seminar, Naval Research Laboratory, Washington, D.C., 21 April 1967
2001	Dynamics of Intense Light Beams in Nonlinear Media	P.L. Kelley	Colloquium, Pennsylvania State University, 9 May 1967

I. SOLID STATE DEVICE RESEARCH

A. CRYSTAL GROWTH, COMPOSITION CONTROL AND JUNCTION FORMATION IN THE LEAD-TIN CHALCOGENIDES

1. Bridgman Crystal Growth of $Pb_{1-y}Sn_ySe$

Single crystals of lead-tin selenide have been grown by the Bridgman technique and have exhibited the same high degree of Pb-Sn ratio homogeneity as reported for $Pb_{1-x}Sn_xTe$ last quarter.[1] The alloy liquid compositions and the corresponding first-to-freeze solid compositions are given in Table I-1 which shows that the Pb-Sn ratio in the solid phase is approximately 0.5 times that of the liquid. The Hall coefficient and electrical resistivity of the crystals cut from the first-to-freeze section of the ingots were measured at 77°K. The carrier concentration and carrier mobility were determined from the results of the electrical measurements. Table I-1 shows that the as-grown crystals were p-type with high hole-carrier densities. Drawing an analogy between these and other lead salt crystals leads to the belief that the excess Se concentration of these Bridgman-grown crystals is greater than the hole-carrier density due to the presence of electrically neutral Se microprecipitates. In order to obtain device grade material, the crystals must be annealed under rather stringent conditions.

2. Isothermal Annealing of $Pb_{1-x}Sn_xTe$ and $Pb_{1-y}Sn_ySe$

Previous studies[1] on the isothermal annealing of $Pb_{1-x}Sn_xTe$ were carried out on single crystal specimens of 1-mm thickness, for annealing times up to 293 hours, and temperatures

TABLE I-1

LIQUID COMPOSITION, SOLID COMPOSITION AND CARRIER CONCENTRATION OF BRIDGMAN-GROWN CRYSTALS OF $Pb_{1-y}Sn_ySe$

Ingot No.	Liquid Composition y	First-to-Freeze Solid Composition y	First-to-Freeze Hole-Carrier Concentration at 77°K (cm^{-3})	Hall Mobility at 77°K (cm^2/V sec)
67-4	0.12	0.064	3.9×10^{19}	220
66-3	0.13	0.074	1.8×10^{19}	1850
67-5	0.14	0.078	2.2×10^{19}	920
67-6	0.16	0.088	4.2×10^{19}	629
67-7	0.18	0.095	5.2×10^{18}	795
67-8	0.40	0.241	3.2×10^{19}	3820
67-3	0.50	0.308	7.0×10^{19}	260

TABLE I-2

RESULTS OF ISOTHERMAL ANNEALING EXPERIMENTS OBTAINED ON BRIDGMAN-GROWN CRYSTALS

Sample Temperature (°C)	Sample Thickness (mm)	Annealing Time (hr)	Carrier Concentration at 77°K (cm^{-3})		Carrier Mobility at 77°K (cm^2/V sec)
Composition $Pb_{0.8}Sn_{0.2}Te$ (metal-rich only)					
750	0.25	21	–		–
650	0.25	additional 43	2.2×10^{18}	p-type	1,350
600	0.25	additional 912	4.3×10^{17}	p-type	1,730
450	0.25	additional 168	1.6×10^{16}	n-type	15,000
Composition $Pb_{0.935}Sn_{0.065}Se$					
Equilibrated with metal-rich powder					
750	1.0	72	7.2×10^{18}	n-type	11,600
650	0.9	120	4.1×10^{18}	n-type	19,300
550	0.26	96	1.8×10^{18}	n-type	18,700
400	–	–	3.36×10^{17}	n-type	26,000
Equilibrated with Se-rich powder					
750	1.0	72	3×10^{19}	p-type	–
650	1.0	168	3.8×10^{19}	p-type	–
550	0.43	312	1.3×10^{19}	p-type	3,100
400	0.012	24	7.1×10^{18}	p-type	2,300

of 650°C to 825°C. In this quarter, $Pb_{1-x}Sn_xTe$ annealing experiments were carried out with a reduced sample thickness of 0.25 mm, longer annealing times and lower annealing temperatures. As shown in the upper section of Table I-2, low concentration p-type and n-type crystals with x = 0.20 were achieved. These results suggest that the solidus line which is in equilibrium with the metal-rich material intersects the stoichiometric composition line at about 465°C for x = 0.20.

The isothermal annealing experiments were extended to the $Pb_{1-y}Sn_ySe$ system. Results for y = 0.065 are summarized in the lower section of Table I-2 which shows that high concentration n-type and p-type material is obtained by isothermal annealing. The n-type sample annealed at 400°C for 84 hours was previously metal-saturated at a higher temperature (650°C). Thus, metal precipitates are possibly present in the crystal. In order to obtain material with low defect and low precipitate concentrations, experiments were carried out using the two-zone annealing technique.

3. Two-Zone Annealing of $Pb_{1-y}Sn_ySe$

By controlling the vapor pressure of Se or of the metal in a second temperature zone, it is possible to achieve a lower defect concentration in the sample at a given temperature than can be achieved by isothermal annealing. Promising crystals for device studies should result by properly adjusting the composition within the solidus field. Our best results with regard to low carrier concentration and high carrier mobility are given in Table I-3. It is seen that carrier concentrations are lower and carrier mobilities are generally higher than the corresponding values obtained by isothermal annealing. However, at the present time, the two-zone annealing results for a given set of annealing conditions are not reproducible. Some possible factors for the non-reproducibility of results are being investigated.

TABLE I-3

TWO-ZONE ANNEALING OF BRIDGMAN-GROWN $Pb_{0.935}Sn_{0.065}Se$ CRYSTALS

Sample Temperature (°C)	Se Temperature (°C)	Sample Thickness (mm)	Annealing Time (hr)	Carrier Concentration (cm^{-3})	Carrier Mobility (cm^2/V sec)
650	160	1.0	144	2.9×10^{17} (n-type)	44,000
650	170	0.44	40	9.0×10^{16} (p-type)	25,000
592	149	0.50	137	1.5×10^{17} (n-type)	42,000
550	130	0.47	312	1.5×10^{17} p-type	25,000
500	100	0.23	360	5.0×10^{16} p-type	20,000

T. C. Harman
A. R. Calawa
Mary C. Finn

B. DIFFUSION STUDIES IN LEAD SALTS

A study of the interdiffusion parameters of Pb and Se in PbSe has been initiated. The technique employed consists of introducing controlled deviations from the stoichiometric concentration of Pb and Se in PbSe.[2] Excess Se in the material makes it p-type while excess Pb makes it n-type. In these experiments excess Se was diffused into n-type and excess Pb into p-type PbSe forming in each case a p-n junction. The material is assumed to be stoichiometric at the junction and the junction depth was measured as a function of diffusion time and temperature.

If the diffusion coefficient is independent of Pb and Se concentration the solution of the diffusion equation can be written as

$$C - C_o = (C_s - C_o)\left(1 - \operatorname{erf} \frac{x}{2\sqrt{Dt}}\right) \tag{1}$$

where C is the excess concentration of the diffusion species in the sample and C_o is the initial excess concentration in the bulk sample. In the present experiments the diffusion species is actually deficient in the bulk sample, such that C_o is a negative number taken to be equal in magnitude to the deficiency in the bulk sample. C_s is the surface excess concentration of the diffused species for the given experimental conditions, x is the distance into the sample, D the diffusion coefficient and t the diffusion time. Since the excess concentration C is taken to be zero at the junction, the diffusion constant D is obtained, once C_s and C_o are known, by plotting the square of the junction depth as a function of the diffusion time.

The experiment consists of placing a p- or n-type sample of known concentration C_o into an evacuated quartz ampule with a Pb- or Se-rich two-phase ingot and heating isothermally. With a two-phase ingot which contains sufficient excess Pb or Se, the surface excess concentration C_s established through the vapor is equal to the saturation concentration at the liquidus-solidus boundary of PbSe at the given temperature. In order to obtain these saturation concentrations at the boundary of the solidus field small samples were equilibrated with an appropriate excess two-phase ingot and quenched to room temperature. The saturation concentrations are shown as a function of temperature in Fig. I-1. These were determined by measuring the carrier concentration in n- and p-type samples. This will give the excess concentration of Pb or Se, considering that each excess Se atom in a lattice site contributes one hole and each excess Pb atom contributes one electron,[3] provided the sample contains no precipitates.

The Pb saturation values obtained in the present work agree quite well with published values;[3] however, the Se saturation values are considerably higher. The latter suggests that considerable precipitation of the Se out of the lattice sites may occur during the cooling process.[4] On the Se side, a temperature is reached above which the samples can no longer be quenched without precipitation. This temperature, about 650°C for these PbSe samples, is reached when the sample cooling rate is comparable to the precipitation rate. The maximum cooling rate is limited by the sample characteristics such as specific heat, thermal conductivity and sample thickness.[5] The thickness of the samples used in these experiments was 2.5×10^{-2} cm.

The initial concentration C_o is equal to the total excess of Pb or Se in the sample including any precipitates. Since there is no direct method of obtaining the precipitate concentration, it is necessary to be certain that the sample contains no precipitates and that the Hall concentration

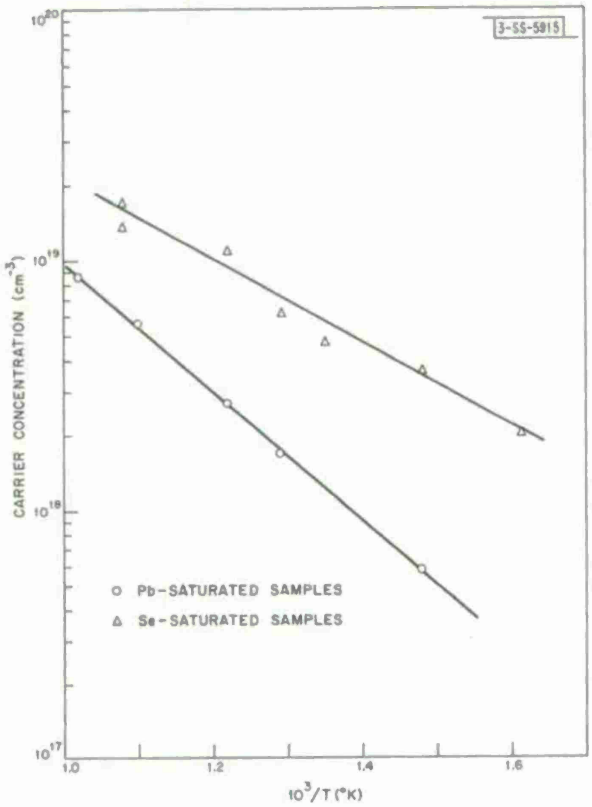

Fig. I-1. Temperature dependence of composition stability limits of Pb and Se in PbSe.

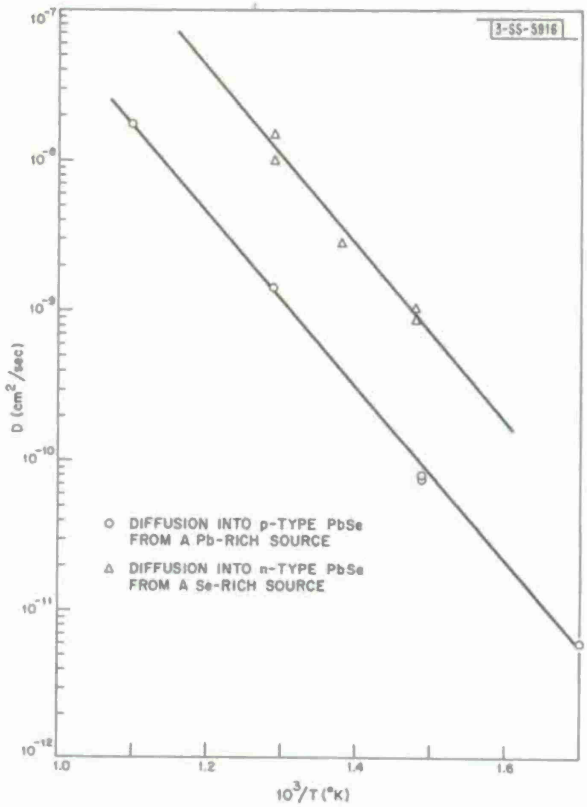

Fig. I-2. Temperature dependence of diffusion coefficient for the interdiffusion of Pb and Se in PbSe.

does indeed represent the total excess of Pb or Se. Knowing the saturation concentrations on both boundaries of the solidus field and the limiting temperature at which samples can be quenched without forming precipitates, an accurate value of C_o can be obtained. The procedure used is to Pb-saturate the samples of as-grown p-type PbSe at about 650°C and quench rapidly. P-type samples are obtained by Se-saturating the n-type material at or below 500°C.

The junction depth is measured by sectioning the sample and thermal probing across the inverted layer. The concentration C at the junction is assumed to be zero. Using an angle-lapping technique and a specially designed microprobe, the junction depth is determined within 1 micron.

The temperature dependence of the diffusion coefficients calculated using Eq. (1) are shown in Fig. I-2. It is noted that the diffusion of excess Se into n-type PbSe proceeds much more rapidly than that of Pb into p-type PbSe. This suggests that the diffusion coefficient is a function of carrier concentration. In the p-type material the initial excess Se concentration ranged from 7×10^{17} cm^{-3} to 1×10^{19} cm^{-3}. Most of the n-type samples had a concentration of about 5×10^{18} cm^{-3}. At least in the range used, the diffusion coefficient does not appear strongly concentration-dependent.

Experiments are now in progress in which both C_o and C_s are varied over a wider range.

A. R. Calawa
P. Youtz
J. Palermo

C. BANDGAP DETERMINATION FROM LASER EMISSION AND PHOTOVOLTAIC RESPONSE MEASUREMENTS IN $Pb_{1-y}Sn_ySe$ DIODES

$Pb_{1-y}Sn_ySe$ lasers and photovoltaic detectors have been fabricated over a wide composition range. Laser action has now been observed out to 18.9 μ and photovoltaic response to 22 μ, both at 12°K. Results show that the energy gap of $Pb_{1-y}Sn_ySe$ varies with Sn content in much the same manner as that of $Pb_{1-x}Sn_xTe$. Lasers and photovoltaic detectors have previously been reported for several compositions of $Pb_{1-x}Sn_xTe$ (Refs. 6 – 8) and a laser for one composition of $Pb_{1-y}Sn_ySe$.[8]

Fabrication methods for all of the lasers were essentially the same as previously described.[8] The lasers exhibit spontaneous emission peaks 2 to 3 meV wide at 12°K. For currents above threshold, characteristic mode structure is observed, with line widths less than 10^{-5} eV. The detectors were fabricated in approximately the same manner as those described in the following section (I-D). No attempt was made to optimize their detectivity.

Positions of emission peaks for $Pb_{1-y}Sn_ySe$ lasers and long wavelength cut-off energies for detectors have been plotted against Sn concentration in Fig. I-3. The abscissa is taken only to y = 0.4 since it is believed that the crystal structure undergoes a transformation at about this concentration. A close agreement is evident between the wavelength of emission and the cut-off wavelength of the photovoltaic response. Hence, the photovoltaic cut-off appears to correspond closely to the energy gap, as was proposed previously for the wavelength of laser

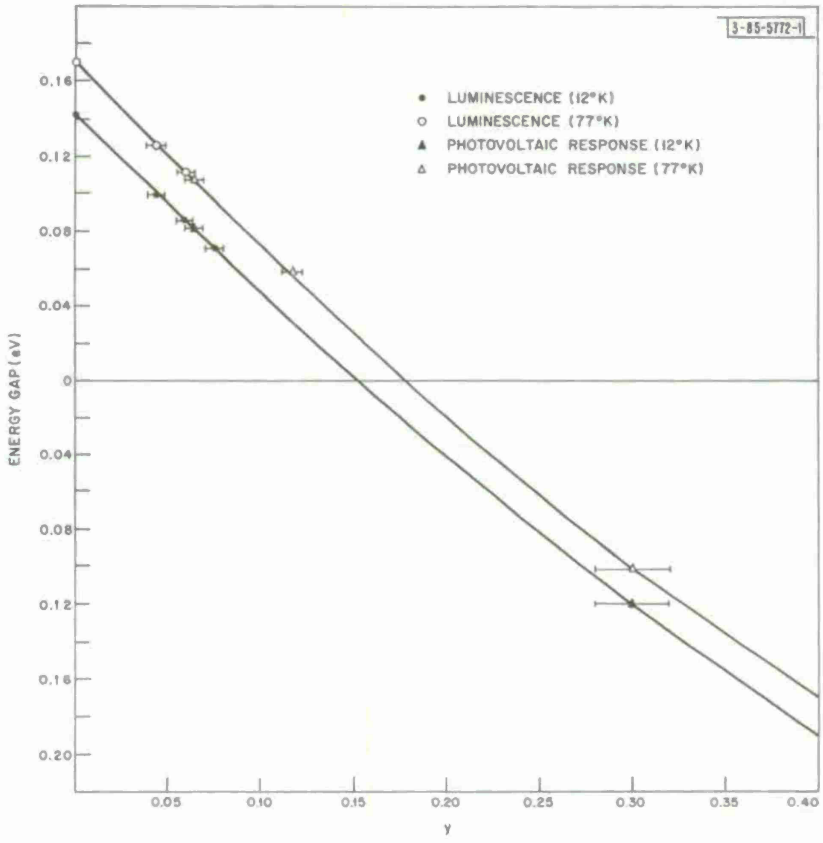

Fig. I-3. Variation of energy gap with composition in $Pb_{1-y}Sn_ySe$.

emission.[6] Note that the temperature dependence of the energy gap of the $Pb_{0.7}Sn_{0.3}Se$ detector is opposite to that of the devices with lower Sn concentration. This reversal is in agreement with a model for the band structure of the $Pb_{1-y}Sn_ySe$ alloys in which the valence and conduction bands cross over at an intermediate composition as was first proposed for $Pb_{1-x}Sn_xTe$. From Fig. I-3 the cross over in $Pb_{1-y}Sn_ySe$ appears to occur at y = 0.15 at 12°K and at y = 0.18 at 77°K. For $Pb_{1-x}Sn_xTe$ the crossover occurs at about x = 0.33 at 12°K and at about 0.37 at 77°K. It was proposed that the composition dependence of the energy gap in $Pb_{1-x}Sn_xTe$ was due largely to the difference in the relativistic corrections for Pb and Sn. If this model is applied to the selenide it predicts a composition dependence of the energy gap in good qualitative agreement with experiment.

J. F. Butler
J. O. Dimmock
T. C. Harman

D. PROPERTIES OF $Pb_{1-y}Sn_ySe$ INFRARED DETECTORS

Efficient photovoltaic detectors of infrared radiation at wavelengths up to 11 μ which operate at 77°K, have been fabricated from annealed Bridgman-grown $Pb_{1-y}Sn_ySe$ crystals.

The structure of a typical detector is shown in Fig. I-4. The wafers are first etch-polished using a KOH etch. A 1000-Å thick SiO_2 layer is then deposited on the surface and 1-mm diameter circular holes are etched in the oxide by means of photo-resist techniques. The SiO_2 layer is deposited on the surface to form a diffusion mask and to passivate the surface at the p-n junction. A 5- to 10-μ n-type layer is then diffused in the oxide-free circular areas of the p-type substrate in a closed-tube process using a crushed metal-rich PbSe ingot as a source. (Alternatively, a p-type layer has been diffused in an n-type substrate using a Se-rich source.) Contact to the n-side is made by evaporating In and contact to the p-side is made by first evaporating a layer of Ag and then a layer of In. The wafer is then cut into square pieces using a wire saw and the pieces are pressure-bonded to a Cu heat sink, which has been In-plated. An In-coated wire is then pressure bonded to the small circular In contact which has been evaporated inside the 1-mm circular area, as shown in Fig. I-4. The heat sink is mounted inside a standard microwave diode package, which has a window cut in the ceramic sleeve for the incoming radiation.

Figure I-5 shows the current-voltage characteristic of a diode at 77°K which was made from a $Pb_{0.936}Sn_{0.064}Se$ crystal. The substrate in this case was p-type with a carrier concentration of about $1.5 \times 10^{17} cm^{-3}$ and a mobility of 26,000 cm^2/V sec.

The slope in the reverse direction corresponds to an impedance of about 5 ohms. The spectral response to this diode at 77°K and at 12°K is shown in Fig. I-6 for the zero bias condition. At 77°K the response peaks at 11 μ, near the 10.6-μ wavelength of a CO_2 laser. This peak, which occurs just prior to the long wavelength cut-off at each temperature, can be attributed to an increase in the number of electron-hole pairs reaching the junction as the radiation begins to penetrate into the material near the bandgap absorption edge.

A large increase in the short wavelength responsivity was observed in these detectors when the thickness of the n-type layer was reduced by etching. The responsivity near the peak of the

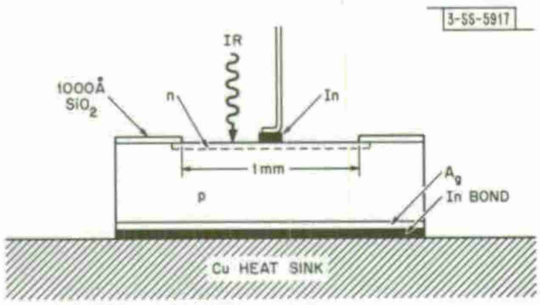

Fig. I-4. Structure of a $Pb_{1-y}Sn_ySe$ detector diode.

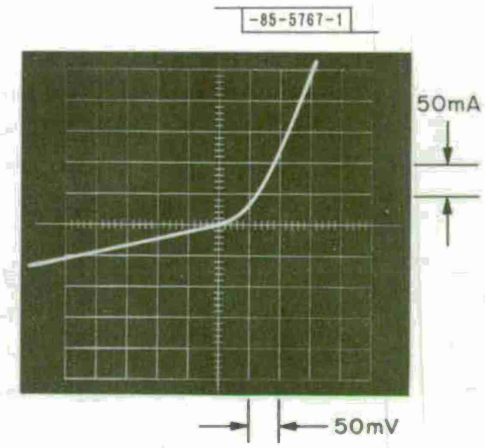

Fig. I-5. Current-voltage characteristics of a $Pb_{0.936}Sn_{0.064}Se$ detector diode at 77°K.

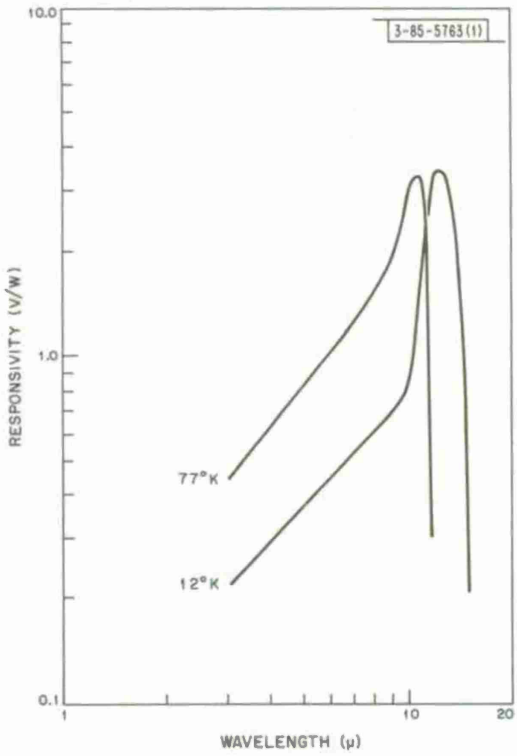

Fig. I-6. Responsivity spectra of a $Pb_{0.936}Sn_{0.064}Se$ detector diode at 77°K and at 12°K.

spectra in Fig. I-6 is about 3 V/W at both temperatures. This value is low because the impedance of the diode, which has an active area of about 1 mm^2, is only about 5 ohms. The external quantum efficiency was estimated to be 10 percent. Since about 50 percent of the radiation is reflected at the surface, this corresponds to a 20 percent internal quantum efficiency.

The detector noise was less than the noise of the measuring system, which yields an upper limit of 10^{-10} V sec. This corresponds to a minimum D^* value of 3×10^9 cm/W $sec^{\frac{1}{2}}$ near the peak at 11 μ. The maximum D^* for a 10 percent quantum efficiency and background-limited operation with a 2π steradian field of view is about 2×10^{10} cm/W $sec^{\frac{1}{2}}$. The risetime of the detector at 77°K was 20 nsec, as measured by observing the response to the output of a pulsed GaAs diode laser. This can be accounted for by the RC constant of the device. The reproducibility of detectors made from the same wafer was essentially 100 percent in terms of cut-off wavelength. The variation in the peak responsivity was no more than 50 percent.

I. Melngailis T. C. Harman
A. R. Calawa W. T. Lindley

E. InSb-GaAsP INFRARED TO VISIBLE LIGHT CONVERTER

A method is proposed and demonstrated by which infrared radiation may be efficiently converted directly to visible radiation by a single solid state device. The device consists of a capacitor-photodetector-photoemitter sandwich in which infrared radiation is incident on one face and the visible radiation is emitted from the opposite face. In order to obtain efficient conversion and allow for a tunable contrast and sensitivity, the low level current produced by the infrared detector is integrated and stored by the capacitor and then delivered to the light emitter in short high-current pulses. The feasibility of such a pulsed device and the efficiencies which may be obtained have been demonstrated using an indium antimonide diode detector and a gallium arsenide-phosphide diode emitter to convert infrared radiation of wavelengths out to 5.3 μ into visible radiation between 0.6 and 0.7 μ.

There have been reports on the use of photoconductors,[9] photodiodes,[10] and phototransistors[11,12] which utilize the photocontrolled discharge of a capacitor to integrate the detected flux for a long time compared to the sampling time. There has also been a report of a solid state device using a Ge-GaAs heterojunction which converts 1.5-μ radiation to 0.9-μ radiation.[13] The work we report here using InSb photodiodes greatly extends the infrared response, uses GaAsP diodes which emit in the visible, and shows that an integration technique enables one to drive light emitters with an improved efficiency.

The circuit we have used involves a capacitor in series with an InSb photodiode and a GaAsP emitting diode. The junction capacitance of the InSb diode can be used for integration, but if this is used in series with light emitters of comparable junction capacitance the integration advantage can be reduced to the point of being ineffective. The structure which involves a metal-oxide-InSb sandwich incorporating a surface depletion region as shown in Fig. I-7 has proven to yield a relatively high capacitance per unit area and a high detection efficiency for large area devices.[14] The capacitance across the oxide has exceeded the effective capacitances of the detector and emitter diodes by an order of magnitude, thus allowing for longer integration times and overcoming limitations imposed by the emitter capacitance.

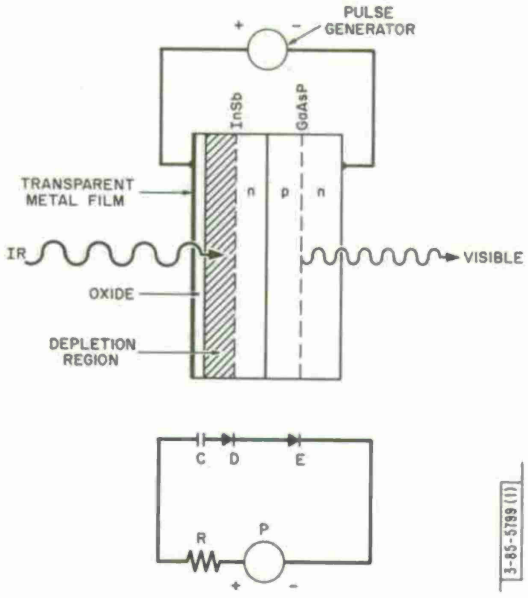

Fig. I-7. Device sandwich structure and equivalent schematic for producing high current driving pulses from low level infrared radiation.

A drawing of a capacitor-detector-emitter sandwich and an equivalent schematic are shown in Fig. I-7. The radiation is incident on the detector through the semi-transparent metal film and oxide layer. During the forward biasing pulses the capacitor C is charged and the emitter E yields pulses of visible light. Between pulses the detector D becomes reverse biased and the capacitor discharge rate, using a low reverse resistance emitter, is controlled by the infrared incident on the detector. Equating the charge removed between pulses to that applied during the forward biasing, one derives a charging current given by

$$i_c = \frac{i_r T_d e^{-t/RC}}{RC\left(1 - e^{-T_c/RC}\right)}$$

where i_r is the detector reverse current, T_d is the discharge interval, T_c is the charging pulse length, and t is the time. This assumes the intervals between pulses are sufficiently short to avoid complete discharge between pulses. If we also assume a short charging time with $T_c \ll RC$, this may be written as

$$\frac{i_c}{i_r} = \frac{T_d}{T_c} \quad .$$

Thus, to have a large ratio i_c/i_r we discharge for a long time T_d and charge for a short time T_c. A more complete analysis leads to the result that the ratio of the change in forward current to the change in detector current has an upper limit given by the ratio of the detector leakage resistance to the series resistance R.

The advantage of converting the low-level detector currents into higher level pulsed currents arises because most diode emitters are much more efficient at the higher current levels. To demonstrate the conversion efficiency and thresholds of detection, we connected in series an emitter diode, an InSb diode detector and a capacitor of 0.01 μF. This value of capacitance corresponds to that obtainable with an oxide layer on the 0.04-cm^2 area of the detector. The emitter had an area of 0.01 cm^2, one-fourth the area of the detector. Using an infrared-generated continuous detector signal of 10 μA to directly drive the emitter, an output of 4×10^{-4} foot-Lamberts (1.4×10^{-7} candles /cm^2) could be obtained; however, using a 100-μsec integration time and 0.1-μsec current pulses, the 10-μA infrared signals were converted to 10-mA driving pulses yielding peak light pulses of 50 fL with an average luminescence of 5×10^{-2} fL, an increase of two orders of magnitude. This, accounting for the 50 percent quantum efficiency of the detector, corresponds to the conversion of an incident 100 μW/cm^2 of 5.3-μ radiation into a signal visible with the unaided eye. The overall quantum efficiency of infrared photons to visible photons was about 10^{-4} and was principally limited by the peak efficiency of the emitter.

In summary, although we have not used the most efficient light emitters, we have shown that the integration technique can be extended to 5.3 μ and used for driving emitters which are relatively efficient only at high current densities. We have shown that it is possible to utilize the large area MOS InSb diodes which incorporate a large series capacitance. Our initial attempts have yielded direct conversion of an infrared level of 100 $\mu W/cm^2$ into light visible to the unaided eye. Much lower infrared levels could be seen by using a visible light intensifier in conjunction with the infrared-to-visible converter. A more complete discussion of the advantages and limitations of using the integration technique to obtain higher emitter efficiencies and to adjust for improved contrast and sensitivity will be given in a future report.

R. J. Phelan, Jr.

F. ELECTROLUMINESCENCE IN CdS

Electroluminescence from CdS vapor-grown platelets has been observed at 4.2°K and 77°K. The high purity platelets* had zero-bias resistivities greater than 10^7 ohm-cm. Indium contacts were usually bonded to opposite faces of the 10- to 20-μ thick samples by heating at approximately 250°C for five seconds in an H_2 atmosphere. Indium contacts have also been applied by pressure bonding at room temperature. Contact areas were generally between 10^{-4} and $10^{-3} cm^2$. The current-voltage characteristics of the devices are as expected for space-charge-limited flow of electrons between closely spaced, planar electrodes.[15] Current densities as high as $2 \times 10^4 A cm^{-2}$ under pulsed conditions and 100 $A cm^{-2}$ DC have been obtained.

At low temperatures, luminescence at the contact edges became evident at about 10 $A cm^{-2}$ DC. The light intensity increased rapidly with current, varying as $I^{3.6}$ over three orders of magnitude in a typical device at 77°K. The external quantum efficiency was between 10^{-6} and 10^{-5} at 1,000 $A cm^{-2}$. Electroluminescence spectra for one sample at 4.2°K and 77°K are shown in Fig. I-8. Relative intensities of the different peaks varied markedly from sample to sample. The highest energy peak at 4.2°K is probably the well known I_1 line.[16] As has been noted by others,[17] this line is extinguished when the temperature is raised to 77°K. The remaining peaks have not been previously classified. The 2.507 eV and 2.469 eV peaks (4.2°K) are separated by the LO phonon energy and, in addition, exhibit the same small shift in energy with temperature. This suggests the lower of these two peaks is a "phonon replica" of the upper.

At present, there is no adequate explanation for the electroluminescence. One speculation is that it results from ionization of electron-hole pairs by hot electrons. The average electric fields are $10^4 V cm^{-1}$ or greater when luminescence is observed. Work will be continued with the aim of clarifying and explaining the effect.

J. F. Butler

G. LASER EMISSION FROM ELECTRON-BEAM-EXCITED ZnTe

Electron-beam-pumped laser emission from ZnTe has recently been reported in the literature.[18] We have independently produced ZnTe lasers by electron beam excitation and have obtained at liquid helium temperature 90-W peak output power with 8 percent overall power efficiency at 5280 Å. Laser action at liquid nitrogen temperature with an emission wavelength of 5310 Å was also observed at somewhat reduced levels of output power and efficiency.

* Supplied by D. C. Reynolds of the Aerospace Research Laboratories.

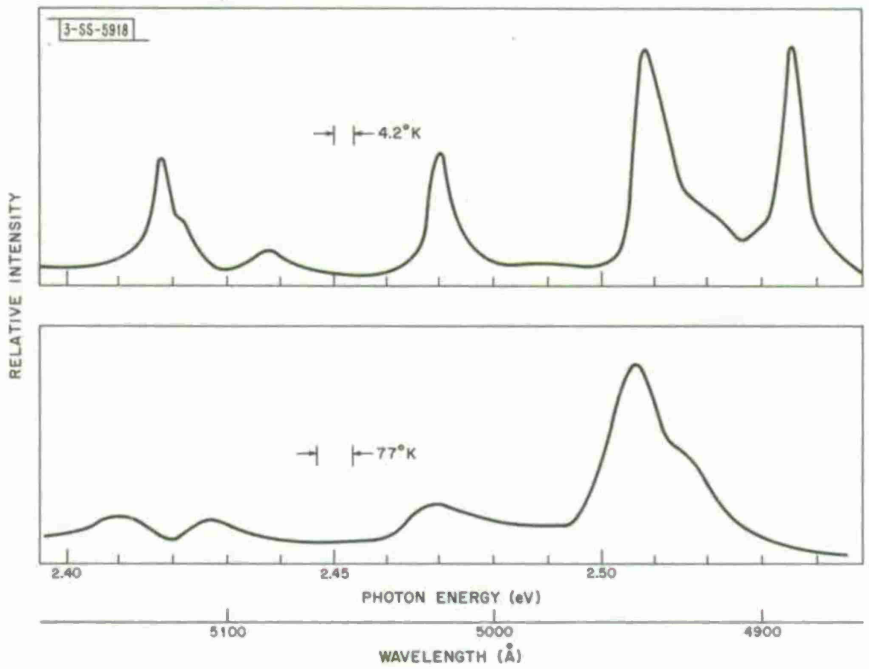

Fig. I-8. Electroluminescence spectra. Current density is 80 A cm^{-2} at 4.2°K and 75 A cm^{-2} at 77°K.

The lasers were made from 10- to 100-ohm-cm p-type ZnTe crystals grown both by closed tube vapor transport using stoichiometric ZnTe powder, and by synthesis from the elements using a Bridgman technique with a Te-rich charge.* Lasers made from crystals grown by the latter method yielded higher output power and efficiency, but the number of crystals of either type examined was insufficient to establish a meaningful pattern. The crystals were ground and chemically polished into (110) oriented plates 50μ thick from which the lasers were then fabricated. A pair of parallel (110) cleaved faces normal to the polished (110) surface formed the 0.5-mm wide Fabry-Perot resonator. One of these cavity faces was coated with a reflective layer of evaporated aluminum. The electron beam was pulsed with 50-nsec pulses at a rate of 60/sec.

A typical set of emission spectra at liquid helium temperature for various levels of excitation is presented in Fig. I-9. Note the scale factors giving the relative emission intensities for the curves. At the lowest beam current the spontaneous spectrum is dominated by a sharp line at 5218 Å which is believed to be due to the radiative recombination of the free exciton.[19] The weak line at 5276 Å most likely results from the recombination of this free exciton with simultaneous emission of a 26-meV LO phonon.[19] In the region between 5220 and 5260 Å there are many closely spaced emission lines which, although weak at low excitation levels, increase in intensity with increasing beam current much more rapidly than does the free exciton line. As noted by Gross et al.,[19] the ZnTe emission bears a strong resemblance to that of CdS, and hence by analogy these latter lines could well be due to recombination of excitons bound to

* The vapor grown crystals were grown by G. W. Iseler and the Bridgman crystals by J. M. Steininger.

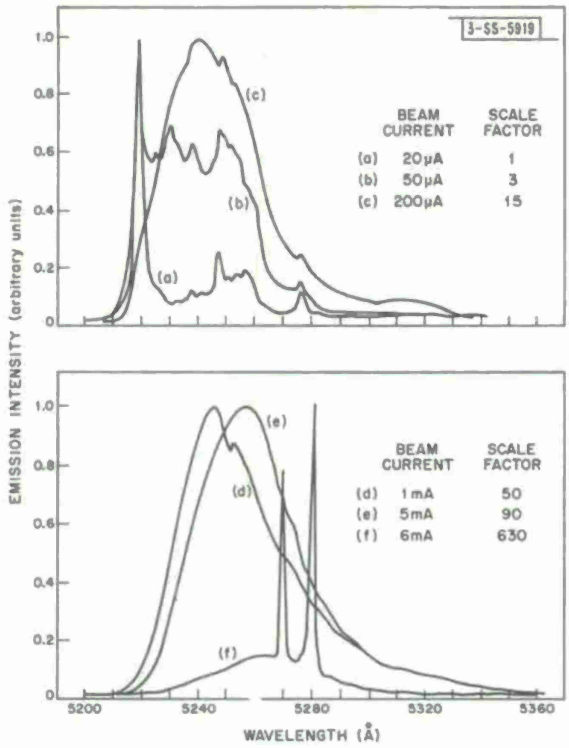

Fig. I-9. Emission spectra of electron-beam-excited ZnTe below [(a) – (e)] and above [(f)] the laser threshold. Beam voltage is 50 kV.

various impurity and/or defect centers. With continued increase in current these lines, in addition to growing rapidly in intensity, appear to broaden until they merge into one broad spontaneous "line" which progressively shifts toward longer wavelengths, presumably due to sample heating. When the laser threshold is exceeded, one or more very intense laser lines appear suddenly on the low-energy side of the spectral peak, as in curve (f) of Fig. I-9. As many as three laser lines with slightly different thresholds have been observed simultaneously in the range from 5260 to 5280 Å. When examined with high spectral resolution each of these lines exhibits the familiar Fabry-Perot cavity mode structure with a mode spacing which corresponds to a value for $(n_o - \lambda_o dn/d\lambda)$ of about 12.

The minimum electron energy for which lasing could be obtained was 48 keV. Over the energy range 48 to 60 keV, the corresponding threshold beam current density for the best sample dropped rapidly from 13 to 4 A/cm^2 at liquid nitrogen temperature and from 6 to 1.5 A/cm^2 at liquid helium temperature. Simultaneously, the output power and power efficiency increased strongly, reaching values with 60 keV excitation of 25 W and 2 percent, respectively, at liquid nitrogen temperature and 90 W and 8 percent, respectively, at liquid helium temperature. Taking into account the energy loss due to backscattering of the incident electrons[20,21] and due to absorption in the evaporated aluminum reflector,[22] one obtains values for the internal power efficiency of about 3 percent and 11 percent at the two temperatures.

The very high values of the laser excitation threshold in ZnTe compared with those observed in similarly excited CdS (Ref. 23) are undoubtedly due in large part to the lower quality of the present bulk ZnTe crystals. In addition, the chemically polished surface upon which the beam impinged was not as flat or smooth as the as-grown platelet faces of the CdS. Improvements in material technology and polishing techniques will hopefully result in a considerable reduction of the excitation threshold for laser emission in ZnTe.

C. E. Hurwitz

REFERENCES

1. Solid State Research Report, Lincoln Laboratory, M.I.T. (1967:1), pp. 6 – 8, DDC 651065.
2. R. F. Brebrick and R.S. Allgaier, J. Chem. Phys. 32, 1826 (1960).
3. N. Ohashi and K. Igaki, Trans. Japan Inst. Metals 5, 94 (1964); H. Gobrecht and A. Richter, J. Phys. Chem. Solids 26, 1889 (1965).
4. R. F. Brebrick and E. Gubner, J. Chem. Phys. 36, 170 (1962).
5. W. Albers, C. Haas and H.J. Vink, Philips Res. Repts. 18, 372 (1963).
6. J.O. Dimmock, I. Melngailis and A.J. Strauss, Phys. Rev. Letters 16, 1193 (1966).
7. I. Melngailis and A.R. Calawa, Appl. Phys. Letters 9, 304 (1966).
8. J.F. Butler, A.R. Calawa, and T.C. Harman, Appl. Phys. Letters 9, 427 (1966).
9. P.K. Weimer, G. Sadisiv, H. Borkan, L. Meray-Horvath, J. Meyer, Jr. and F.V. Shallcross, International Solid-State Circuits Conference, Philadelphia, Pa., Feb. 10, 1966.
10. G.P. Weckler, International Electron Devices Meeting, Washington, D.C., Oct. 20 – 22, 1965.
11. G.P. Weckler, International Electron Devices Meeting, Washington, D.C., Oct. 26 – 28, 1966.
12. G. Strull and D.H. McCann, International Electron Devices Meeting, Washington, D.C., Oct. 26 – 28, 1966.
13. P.W. Kruse, F.C. Pribble, and R.G. Schulze, Bull. Am. Phys. Soc. 12, 275 (1967).
14. R.J. Phelan, Jr. and J.O. Dimmock, Appl. Phys. Letters 10, 55 (1967).
15. M.A. Lampert, Proc. I.R.E. 50, 1781 (1962).
16. D.G. Thomas and J.J. Hopfield, Phys. Rev. 128, 2135 (1962).
17. C.E. Bleil and I. Broser, Physics of Semiconductors (Dunod, Paris, 1964), p. 897.
18. A.N. Vlasov, G.S. Kozina, and O.B. Fyodorova, Zh. Eksp. Teor. Fiz. 52, 434 (1967).
19. E.F. Gross, L.G. Suslina, and A.I. Livshits, Fiz. Tverd. Tela 5, 801 (1963).
20. E.J. Sternglass, Phys. Rev. 95, 345 (1954).
21. J.E. Holliday and E.J. Sternglass, J. Appl. Phys. 28, 1189 (1957).
22. L. Holland, Vacuum Deposition of Thin Films (Wiley and Sons, Inc., New York, 1958), p. 322.
23. C.E. Hurwitz, Appl. Phys. Letters 9, 420 (1966).

II. OPTICAL TECHNIQUES AND DEVICES

A. CO_2 LASER RADAR SYSTEM

A continuous-wave CO_2 laser has been adapted for use in an exploratory Doppler-type laser radar system operating at a wavelength of 10.6 μ. This system is being used to evaluate components and techniques for applying infrared laser devices to the problems of precision velocity and position determination of moving objects. Presently, it is capable of measuring radial velocities and automatic tracking of moving objects such as automobiles and pedestrians. Modifications on the system now in progress are expected to allow tracking of low-flying aircraft in the vicinity of the Laboratory; the system has been installed in a temporary shelter on the roof of one of the Laboratory buildings. The laser is kept stationary, with beam pointing accomplished by a plane mirror on a small radar-type pointing mount located on the roof of the shelter. In order that orthogonal motions of the mount produce orthogonal motions of the beam for any position of the mount, it is necessary that the laser beam be brought onto the mirror along the mount's azimuth axis. This requirement was met by inverting the pointing mount on the roof above the laser beam and bringing the beam vertically upward onto the mirror. The principal disadvantage of this method arises from obscuration of the zenith; however, this is not a serious limitation since the azimuth-elevation mounts are not useful close to zenith.

The radar system is based on heterodyne detection of a reflected laser beam which has been shifted in frequency by a moving object in proportion to the relative velocity of the object. The frequency-shifted return beam is combined with an upshifted sample of the laser output on a fast square-law detector. The output of the detector then includes a signal, occurring at the difference frequency of the two mixed beams, which is also proportional to the velocity of the moving object. Doppler frequency shifts for reflected radiation are given by $\Delta f = 2(v/\lambda)$, which is equivalent to about 85 kHz/mile/hour. Thus, moving automobiles and low-flying aircraft are observed at frequencies below 20 MHz. Figure II-1 is a drawing of the radar system layout showing the laser source, interferometer, beam expander, and pointing mount locations.

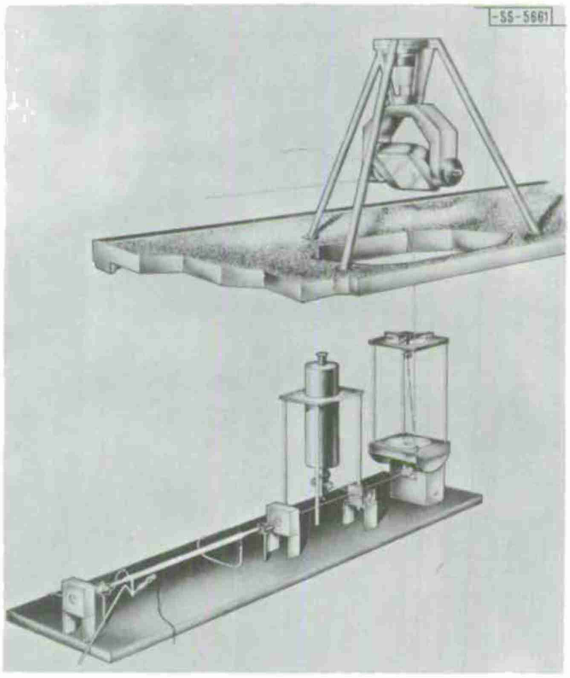

Fig. II-1. Laser radar system. Principal components are shown in their relative positions.

Copper-activated germanium photoconductors, produced at Lincoln Laboratory, have

Fig. II-2. Return signal from moving automobile displayed on spectrum analyzer. Entire trace corresponds to frequency shifts of 1 MHz. Signal is seen near 100 kHz. At left is zero frequency response of analyzer.

sufficiently fast response for use in this frequency region. Teich, et al.,* demonstrated that these photoconductors are capable of heterodyne detection of 10-μ radiation close to the theoretical limit of $(2h\nu/\eta)$ B when operated at liquid helium temperature.

The pointing mount has been provided with three modes of beam direction: a position servo loop for fixed directions, a "joystick" rate control for manual tracking, and an auto-track control loop using detected laser return signals. A closed-circuit vidicon camera has been boresighted to the laser beam axis in order to facilitate target acquisition and manual tracking. At present, the auto-track mode is an elementary form based on detection of broad-band return signals. This method will soon be replaced by a narrow-band variable frequency method which will permit tracking on smaller signals than may be used with the broad-band method. Doppler return signals have been observed from objects up to 2 miles from the Laboratory. An example of the return signal from a slow-moving automobile displayed on a spectrum analyzer is shown in Fig. II-2. The radial velocity is approximately $1\frac{1}{4}$ miles per hour.

H. A. Bostick

B. SEALED CO_2 LASER TUBE WITH GREATER THAN A 700-HOUR LIFE

Work has continued with a CO_2 laser tube that is similar to the tube discussed in the last Solid State Research Report.† The difference between this tube and the tube reported on was in the choice of Ni rather than Kovar for the cathode metal. Adsorption at the cathode of the carbon-oxygen compounds made the choice of metal type a critical one, and Ni was chosen because its reactions with these compounds was likely to be reversible. Figure II-3 shows the concentrations, indicated as pressures, of the molecules that were in the tube versus operating time. The concentrations were determined by mass analyzing gas samples taken from the operating tube. Only CO and O_2 were formed in concentrations comparable to the concentration of the initial fill gases of 2 torrs CO_2, 2 torrs N_2, and 7 torrs He. No nitrogen-oxygen compounds seemed to be found other than at impurity concentrations. After the initial adsorption within 335 hours of operation, the gases were easily desorbed when the cathode temperature was raised to 300 °C. When the CO_2 was adsorbed to a pressure of 0.2 torr the laser output power dropped to zero; but when the desorption was complete with a redemption of 80 percent of the CO_2, the output power was

*M. C. Teich, R. J. Keyes and R. H. Kingston, Appl. Phys. Letters 9, 357 (1966).

†Solid State Research Report, Lincoln Laboratory, M.I.T. (1967:1), DDC 651065.

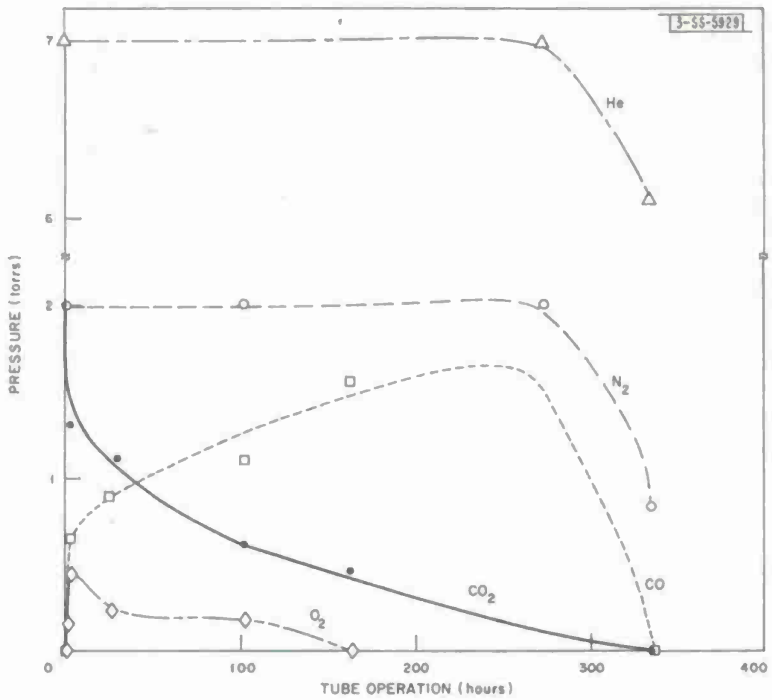

Fig. II-3. Partial pressures of CO, O_2, CO_2, N_2 and He in laser tube shown as a function of operating time.

resumed at its initial value. The adsorption-desorption process was cycled several times up to 709 hours continuous operation with a resumption of normal laser power output, and at this time 80 percent of the original fill of CO_2 was still being reclaimed. At the 709-hour point, the pressures of the major constituent gases were established as 1.7 torrs CO_2, 1.2 torrs N_2, 0.25 torr CO, 7 torrs He, 0.03 torr O_2, and the major impurity of H_2 at 0.48 torr. Inadvertently, water was dropped on one Brewster NaCl window destroying its optical flatness and the tube ceased lasing at this time.

It seems that the CO_2, CO, and O_2 interacted with the Ni and NiO and carbon surfaces forming a carbonate, $CO_3^=$ complex, on the surfaces which was desorbed as CO_2 and CO when the cathode region was heated. The carbon was most likely formed in the sputtering process while the NiO was formed with the free oxygen or an oxygen complex on the sputtered Ni film. The specific power generation of 0.15 W/cm^3 for this 10 mm bore laser was not too far different from the 0.25 W/cm^3 generated in a flowing gas tube of the same diameter, and the difference could be due to the higher concentration of CO and O_2 and the higher gas temperature in the sealed tube versus the flowing tube.

R. J. Carbone

C. PHOTOVOLTAIC HETERODYNE DETECTION IN $Pb_{1-x}Sn_xSe$

A $Pb_{1-x}Sn_xSe$ photovoltaic detector has been employed to observe heterodyne detection, using scattered radiation from a CO_2 laser as a signal at 10.6 μm. The observed minimum detectable power, at a frequency of 110 kHz and in a bandwidth of 65 kHz, was 1.8×10^{-14} watt, which is to be compared with the theoretical value of 1.7×10^{-14} watt. At these low frequencies, present

photovoltaic devices perform as well as Ge:Cu photoconductive detectors, and have the distinct advantage of operation at 77 °K rather than at 4 °K. Work is now being directed toward operation at higher frequencies and in wider bandwidths.

M. C. Teich

D. FARADAY ISOLATOR

Faraday rotation and absorption have been measured at 10.6 μm in InSb in order to construct an isolator for the CO_2 laser. Sufficient rotation to obtain isolation (45 °) has been obtained in a 0.5-mm thick sample with a carrier concentration of 2.3×10^{17} cm^3, and a mobility of 45,000 cm^2/V sec at 5200 gauss. The sample absorbs 10 percent of the beam energy. The isolation capability of the device will be limited by the uniformity of the field and the performance of the polarizer. The power handling capability will be limited by the thermal conductivity of the material. Work is in progress to determine these limitations.

Jane H. Dennis

III. MATERIALS RESEARCH

A. CRYSTAL GROWTH

1. $MnBr_2$

Crystals of $MnBr_2$ have been grown from the vapor phase and from the melt by a method similar to the one used to obtain MnI_2 crystals.[1] Helium was saturated with bromine vapor by bubbling it through liquid bromine at 0°C, and then passed over a quartz boat containing manganese powder heated to 850°C at the entrance to a muffle furnace with a decreasing temperature gradient. Under these conditions the Br_2 and Mn reacted to form $MnBr_2$ vapor. Most of this vapor condensed at temperatures above about 700°C as a liquid which solidified on cooling to form large transparent grains about 3 mm thick. The balance of the $MnBr_2$ vapor condensed in a cooler region of the furnace as single crystal platelets of which the largest was about 2 × 2 × 0.005 cm. It was found that $MnBr_2$ is considerably less hygroscopic than MnI_2, and can be exposed to the atmosphere for several days before deteriorating.

T. B. Reed
W. J. LaFleur

2. EuO

A large-grained ingot of EuO, an infrared-transparent ferromagnetic material, has been obtained by a modification of the method described by Guerci and Shafer.[2] The ingot was prepared from a nonstoichiometric melt in a molybdenum crucible 7 cm long, with an outside diameter of 3 cm and a maximum inside diameter of 1 cm. The inner chamber was tapered to permit easy removal of the ingot. The crucible was loaded with 3.0 g of Eu metal and 3.5 g of Eu_2O_3, corresponding to a composition of $Eu_{1.33}O$, and then sealed to prevent vaporization losses by means of a deformable molybdenum washer held in place by a threaded cap. The charge was heated in a resistance furnace to 2000°C for 1 h, cooled to 1100° at the rate of 9°C/h, and then cooled rapidly to room temperature. The dark-red ingot formed was 1.5 cm long and contained single crystal grains up to 4 mm across. A sample from the ingot gave a Debye-Scherrer pattern containing only lines of the fcc EuO phase. The lattice parameter a_o determined from this pattern is 5.1438 ± 0.004 Å, compared with literature values of 5.1451 ± 0.0003 Å (Ref. 2) and 5.1439 Å (Ref. 3).

T. B. Reed
R. E. Fahey
E. R. Pollard

B. KINETICS OF ELECTRON TRANSFER BETWEEN CONDUCTION BAND AND SULFUR DONORS IN GaSb

At atmospheric pressure, the lowest sulfur donor level in GaSb lies about 0.075 eV below the lowest conduction band, which has Γ_1 symmetry. Measurements of resistivity as a function of pressure[4] have shown that this donor level is associated primarily with the X_1 conduction band minima, which lie at an energy estimated to be about 0.3 to 0.4 eV above the Γ_1 minimum.

At temperatures below about 100°K, nonequilibrium effects were observed in resistivity and Hall coefficient measurements on S-doped GaSb.[5] These observations indicated that the rate at which electrons are transferred from the conduction band to the sulfur donor levels decreases so rapidly with decreasing temperature that it becomes readily observable in the vicinity of 100°K. A series of isothermal measurements has been made to determine the temperature dependence of the transfer rate. In each experiment the sample was first cooled from room temperature by plunging it into a mixture of liquid oxygen and liquid nitrogen in the correct proportions to give the desired temperature, and the resistivity was then measured as a function of time. When the sample reaches the bath temperature, its resistivity has increased by about two orders of magnitude due to the deionization of the sulfur donors, but the concentration of electrons in the conduction band still exceeds the equilibrium concentration. Therefore the resistivity slowly increases to its equilibrium value as electrons fall from the conduction band into empty donor levels.

The results for a typical experiment, conducted at 90.2°K, are shown in Fig. III-1. In order to facilitate analysis, the data are presented in terms of conductivity rather than resistivity. In particular, the difference between the conductivity at a given time and the final, equilibrium conductivity is plotted logarithmically versus time. Since it was found that the electron mobility at constant temperature does not change significantly with carrier concentration, the conductivity difference $\Delta\sigma$ is proportional to the difference between the instantaneous carrier concentration and the equilibrium concentration. At each temperature the results can be represented

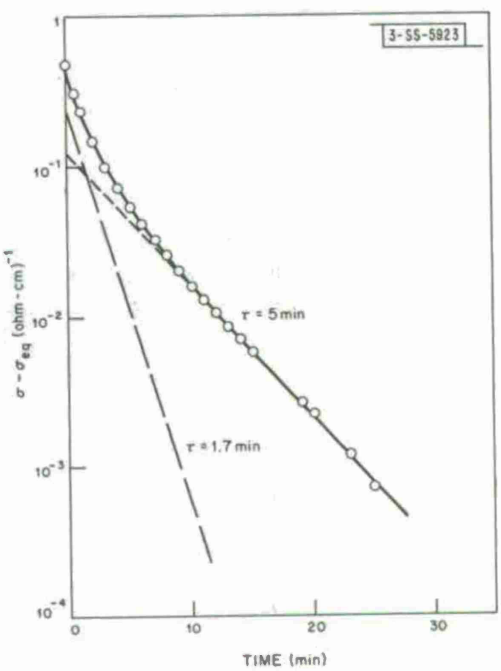

Fig. III-1. Time dependence of electrical conductivity at 90.2°K for S-doped GaSb sample which was cooled very rapidly from room temperature.

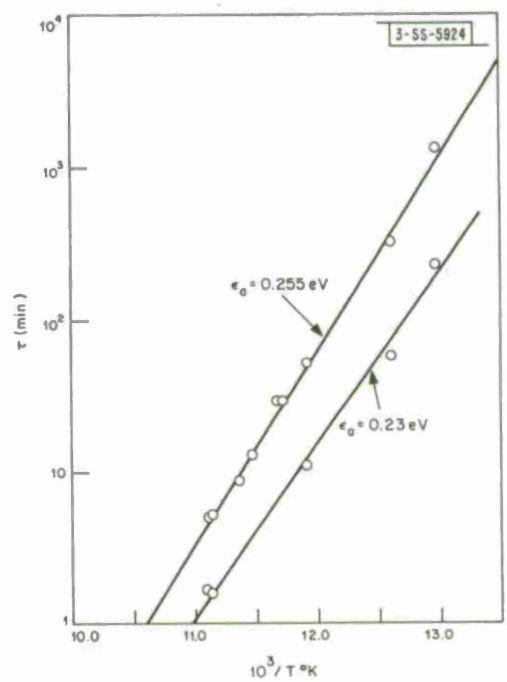

Fig. III-2. Temperature dependence of time constants for transfer of electrons from the conduction band to the sulfur donor levels in S-doped GaSb.

satisfactorily as the sum of two straight lines corresponding to two different time constants defined by the expression $\Delta\sigma = A \exp(-t/\tau_1) + B \exp(-t/\tau_2)$.

The temperature dependence of the two time constants is shown in Fig. III-2, where the logarithm of τ is plotted against reciprocal absolute temperature. The slower time constant increases from 5 min. at 90°K to 1300 min. at 77°K, and the faster time constant increases from 1.6 to 230 min. over the same temperature range. Both constants vary exponentially with reciprocal temperature, since the data are well represented by two straight lines. The activation energies calculated from the slopes of these lines are 0.255 eV for the slower time constant and 0.23 eV for the faster one. These energies may be regarded as the same within the limits of experimental error.

Nonequilibrium effects like those described have not been reported previously for GaSb nor any other pure III-V compound, although quite similar observations have recently been made on S-doped $GaAs_{1-x}P_x$ alloys.[6] At low temperatures, the conduction electrons in the GaSb samples are almost entirely in the Γ_1 conduction band. Since the lowest sulfur donor levels are associated primarily with the X_1 conduction band, it seems possible that the cross section for scattering from a Γ_1 state to an X_1 state might be small enough to account for the observed transfer rates. No attempt has been made to calculate this cross section theoretically. It should also be noted that an explanation for the two different time constants characterizing the decay of conduction electrons is not obvious on the basis of this model.

G. W. Iseler
A. J. Strauss

C. POLYMORPHISM IN Ag_2Te AT HIGH PRESSURES AND TEMPERATURES

Previous electrical resistivity and x-ray diffraction studies on Ag_2Te revealed the existence at room temperature of two high-pressure phases, one stable between about 22 and 25 kbars and the other stable above 25 kbars (Ref. 7). In order to obtain further data on the boundaries of these phases, additional resistivity measurements have been made as a function of temperature and hydrostatic pressure. The results obtained have been used to construct the partial P-T diagram for Ag_2Te shown in Fig. III-3, where the high-pressure phases are designated as Ag_2Te-II and Ag_2Te-III.

Since the transition points shown in Fig. III-3 were located by changes in the slope of resistivity curves measured as a function of temperature (isobars) or pressure (isotherms), the accuracy of these points depends on the abruptness of the changes in slope. For the I → II and II → III transitions, the changes are quite sharp at room temperature but become increasingly gradual above 50°C. Therefore the I-II and II-III phase boundaries are shown as dashed lines in Fig. III-3. There is some indication that these two boundaries intersect at some temperature below the boundary of the f.c.c. phase.

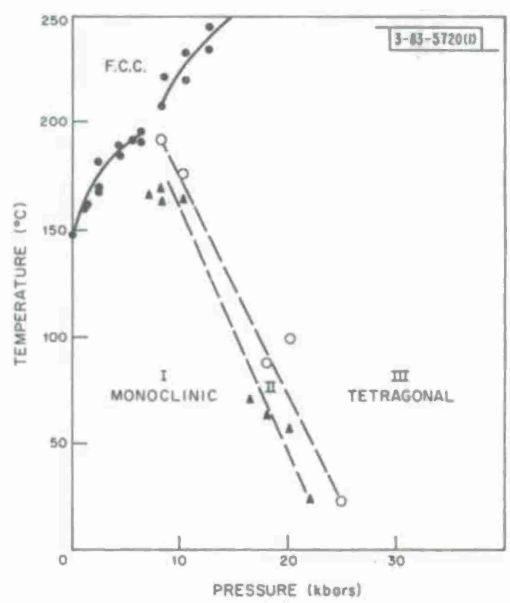

Fig. III-3. Pressure-temperature diagram for Ag_2Te.

The crystal structure of Ag_2Te-III has been determined from x-ray diffraction patterns obtained with a new diamond-squeezer high-pressure unit designed by Bassett.[8] This apparatus has two principal advantages: the x-ray beam is finely collimated and precisely centered on the face of the piston diamond, and the sample while under pressure can be observed through the anvil diamond with a metallographic microscope. These features are important because in this type of equipment the pressure is highest at the center of the piston face and decreases markedly toward the periphery. Consequently, in many cases more than one phase is present. Since various phases differ in their reflectivity, both for polarized and unpolarized light, with the Bassett camera their locations can be determined visually. Therefore it is possible to see whether the pressure can be adjusted so that the entire area of the x-ray beam is intercepted by a single phase, as required for an unambiguous diffraction pattern. This could be done for Ag_2Te-III, as shown by the high-pressure photomicrograph of Fig. III-4. The dark area in the center is Ag_2Te-III, the adjacent lighter area is Ag_2Te-II, and the dark ring at the periphery of the piston is the atmospheric pressure monoclinic phase.

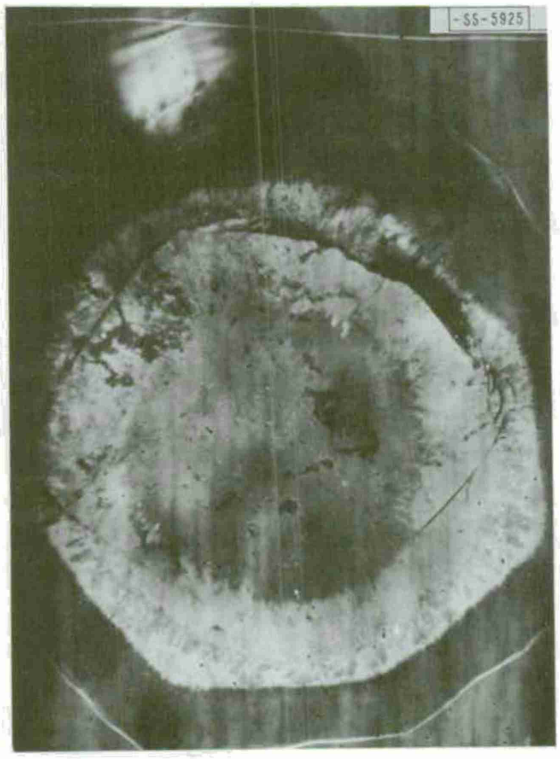

Fig. III-4. Photomicrograph of Ag_2Te sample under pressure in Bassett x-ray camera, showing concentric areas of Ag_2Te-III (center,) Ag_2Te-II, and Ag_2Te-I (outside).

The x-ray pattern for Ag_2Te-III has been indexed on a tetragonal cell with a = 8.80 Å, c = 6.20 Å, and c/a = 0.71. The hkℓ values assigned to the diffraction lines, together with the observed and calculated d-spacings for this indexing, are given in Table III-1. The calculated density at pressure is 9.5 g/cm^3, assuming 8 molecules per unit cell. This corresponds to a density increase of 13 percent with respect to the monoclinic phase at one atmosphere.

TABLE III-1

INDEXING OF X-RAY PATTERN FOR HIGH-PRESSURE Ag_2Te-III (TETRAGONAL)

hkℓ	d-spacing (Å)		Intensity
	Observed	Calculated	
221	3.31	3.32	1
300	2.93	2.93	10
221,112	2.74	2.77	4
311,202	2.54	2.54	8
320	2.40	2.44	2
321	2.25	2.27	0.5
400	2.20	2.20	4
302	2.13	2.13	1
312,330	2.08	2.07	5
331,103	1.98	1.97	1
203	1.88	1.87	1
402	1.80	1.79	< 0.5
431	1.69	1.69	4
511	1.65	1.66	< 0.5
400	1.55	1.56	1
600	1.48	1.47	3
611	1.41	1.41	2
630,602	1.31	1.31	5
622	1.27	1.27	1
720	1.20	1.21	3

The structure of Ag_2Te-III appears to be isotypic with that of Ag_2S (Ref.9). The ratio of the unit cell volumes for the two compounds (1.37) is approximately equal to the ratio of the atomic volumes for tellurium and sulfur (1.32). The space group has not been determined for either structure.

As shown in the P-T diagram of Fig. III-3, Ag_2Te-II is stable only over a rather narrow pressure range. For this reason it has not been possible with the Bassett camera to obtain an x-ray diffraction pattern which is due entirely to Ag_2Te-II. In order to determine the structure of this phase, its diffraction pattern will be found by subtracting the known lines of Ag_2Te-I and Ag_2Te-III from composite patterns for Ag_2Te-I + Ag_2Te-II and for Ag_2Te-II + Ag_2Te-III.

M. D. Banus
Mary C. Finn

D. EFFECT OF HIGH PRESSURE ON OXIDES WITH DEFECT-ROCKSALT STRUCTURES

The monoxides of Ti, V, and Nb are compounds which contain unusually large concentrations of lattice vacancies, located at both metal and oxygen sites. For the Ti and V oxides, the range of homogeneity is quite wide, with x between 0.8 and 1.25 for TiO_x. Up to 15 percent of all sites are vacant. When prepared by the usual methods, these two compounds have the rocksalt (B1) structure, with the vacancies randomly distributed through the lattice. (Ordered structures can also be prepared by prolonged annealing at sufficiently low temperatures.) For NbO_x, the range of homogeneity is much narrower ($0.98 < x < 1.03$). In this case, 25 percent of the sites are vacant, and the vacancies are ordered to give a structure which is different from B1, but related to it.

A study is being made to determine whether the concentration of vacancies in the three monoxides can be significantly reduced by the application of high pressures. Most of the experiments so far have been made on polycrystalline TiO_x ingots obtained by quench casting of melts prepared by arc melting mixtures of crystal bar Ti and high purity TiO_2 in appropriate proportions. These samples are significantly higher in purity than those we have made by other methods. The stoichiometry is determined gravimetrically by measuring the weight gain on combustion to TiO_2. The x-ray density is calculated from the cubic lattice parameter a_o determined from the diffraction pattern obtained with a Debye-Scherrer camera. The a_o values are accurate to ±0.001 Å for good films and to ±0.003 Å for poorer ones. The measured density is found with a micropycnometer, using toluene as the pycnometric fluid. The concentrations of Ti and O vacancies are then calculated by comparing the x-ray and measured densities according to the method described in the literature.[10,11]

In a typical experiment, the TiO_x sample is first annealed for ~ 20 hours at 1500°C in vacuum or under argon at about 500 torrs. After the x-ray and pycnometric measurements are made, a portion of the sample is annealed for 1 to 3 hours at about 50 kbars and 1100 to 1300°C, and the densities are again measured. Representative results for samples with x between 0.87 and 1.06 are given in Table III-2. In every case annealing under pressure caused a decrease of at least 15 percent in the calculated total vacancy concentration. The magnitude of the decrease appears to depend more on the purity and stoichiometry of the material than on the pressure, temperature, and time of anneal. Application of pressure caused an increase in a_o, which resulted in a decrease in the x-ray density although the measured density increased. The increase in a_o is due to the decrease in vacancy concentration, since the effect of a large concentration of randomly distributed vacancies is to decrease the apparent average bond length and therefore the size of the unit cell.

The data in Table III-2 also show that the reduction in vacancy concentration was accompanied by an increase in the superconducting transition temperature T_c for TiO_x. For samples prepared at atmospheric pressure it has been reported[12] that T_c varies strongly with x, reaching a maximum of about 1°K for x = 1.0. Since the lower limit of measurement in the present experiments is about 1.2°K, no superconducting transition could be observed in vacuum-annealed samples. After annealing under pressure, most of the samples had transitions between 1.3 and 1.8°K, although in some cases a well-defined T_c could not be determined because the transitions

TABLE III-2

EFFECT OF PRESSURE ON TiO_x

x	Treatment	a_o (±0.001) (Å)	X-ray Density (g/cm^3)	Pycnometric Density (g/cm^3)	Fraction of Sites Occupied		Total Vacancies (percent)	Decrease in Vacancies (percent)	T_c (°K)
					Ti	O			
0.872	A*	4.190	5.580	5.043	0.904	0.788	15.4	17	<1.25
	B†	4.200	5.544	5.162	0.931	0.812	12.8		~1.3
0.934	A	4.190	5.673	4.977	0.877	0.819	15.2	27	<1.20
	B	4.200	5.633	5.171	0.919	0.858	11.1		~1.6
0.999	A	4.185	5.788	4.926	0.851	0.850	15.0	15	<1.3
	B	4.192	5.729	5.021	0.872	0.871	12.8		1.4
1.060	A	4.179	5.902	4.936	0.836	0.886	13.9	15	<1.3
	B	4.194	5.838	4.998	0.856	0.907	11.8		~1.8

* Annealed under vacuum at 1550°C.

† Sample A, annealed at ~50 kbars and 1100°C.

were too broad. (It should be noted that samples low in carbon and nitrogen content are required for meaningful superconductivity experiments in TiO_x, since mixtures with TiN and TiC have relatively high T_c's.)

Annealing experiments similar to those described for TiO_x have also been performed on several samples of NbO_x. Application of pressures up to 90 kbars caused no detectible change in either a_o or measured density. This result is not surprising, since the presence of a large concentration of ordered vacancies apparently stabilizes the NbO_x lattice.

M. D. Banus

E. EFFECT OF HYDROSTATIC PRESSURE ON THE CURIE POINT OF $SrRuO_3$

A nonmagnetic pressure vessel, made of beryllium-copper, has been constructed for studies on the effect of hydrostatic pressure on magnetic susceptibility. This unit is small enough in diameter to fit into the dewar used with a vibrating coil magnetometer. The vessel is connected to a high-pressure gas apparatus capable of developing pressures up to 14 kbars. Use of helium gas as the pressure transmitting medium permits susceptibility measurements to be made at low temperatures.

The new equipment has been used to investigate the pressure dependence of the Curie temperature (T_c) of $SrRuO_3$, a ferromagnetic compound whose T_c is about 164°K at atmospheric

pressure. Over the range from atmospheric pressure to 6 kbars, the limit of the measurements, T_c was found to decrease linearly with increasing pressure at the rate of 0.63°K/kbar. This reduction in T_c supports the hypothesis[13] that the magnetic properties of $SrRuO_3$ are primarily due to band effects rather than to localized moments.

J. A. Kafalas K. Dwight
N. Menyuk J. B. Goodenough

F. ELECTRON DENSITY DIFFERENCE MAP AS FURTHER EVIDENCE FOR TRAP-MEDIATED Pb-Pb BOND IN $PbRuO_3$

The existence of a trap-mediated Pb-Pb bond in $PbRuO_3$, a compound with pyrochlore structure, has been proposed on the basis of a structure refinement which indicated that oxygen vacancies at the 8(b) sites in the lattice act as traps for electrons transferred from the four Pb ions which are arranged tetrahedrally around each of these sites.[14] Evidence supporting this model was obtained by comparing the ionic radius of Pb in this compound with its radii in other materials with pyrochlore structure.

In order to obtain more direct evidence concerning the proposed model, an electron density difference map has been calculated for $PbRuO_3$. To obtain this map, a Fortran computer program was written to generate electron density maps from structure factors for x-ray scattering. This program was used to obtain theoretical electron distributions in $PbRuO_3$ from the form factors for O^{2-} (Ref. 15), Pb^{2+}, and Ru^{4+} (Ref. 16) and the known positions of Pb, Ru, and O in the compound. Since the atom positions and space-group were known, the values of the phase angle α could be obtained from the same theoretical form factors. (Although the structure is

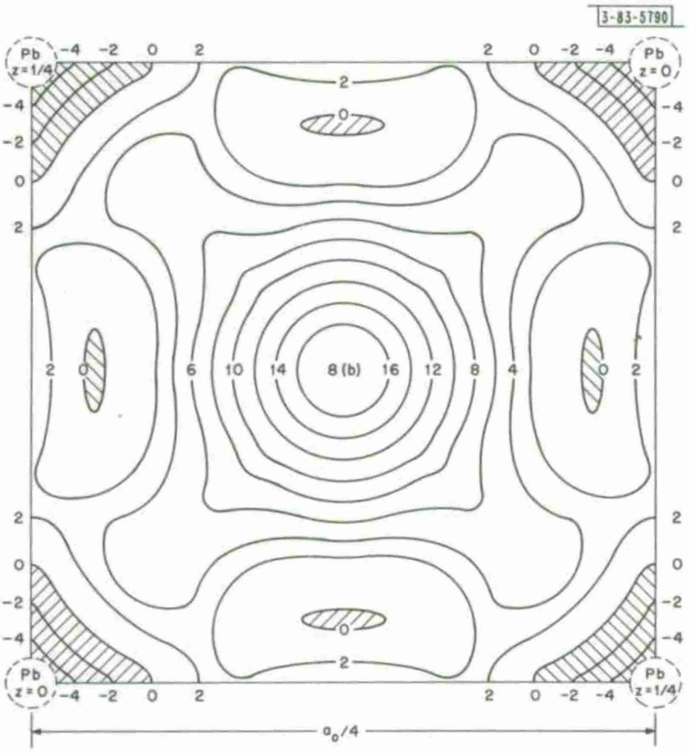

Fig. III-5. Electron density difference map for $PbRuO_3$, for a section at z = 0.125 parallel to the (001) planes.

centrosymmetric, values of α as different from 0 and π as 0.2 and 2.8, respectively, were obtained because of the contribution of the imaginary part of the correction for anomalous dispersion. If this term had been neglected, the calculations would not have been of sufficient accuracy.) The same Fortran program was used to compute experimental electron distributions from the structure factors calculated from integrated x-ray intensity data for $PbRuO_3$. Wherever reflections overlapped, the contribution of the individual structure factors was deduced from the theoretical ratios. Including all the positive and negative permutations, summations were made for 1242 (hkℓ) combinations.

In order to investigate the whole cell, electron density maps were obtained for three two-dimensional sections, parallel to the (001) plane, located at z = 0, 0.125, and 0.25. Analysis of these maps showed that 2.0 ± 0.3 electrons were transferred from each of the lead atoms. A Fourier difference map, showing the difference between the theoretical and experimental electron distributions, was then made for the section at z = 0.125, as shown in Fig. III-5. This map shows unambiguously that the electrons transferred from the lead atoms are located at the 8(b) site, thus confirming the proposed model of a trap-mediated Pb-Pb bond. Two features of the map are particularly interesting: (1) the large volume required for the trapped electrons because there is no positive potential at the 8(b) site, and (2) the tetrahedral symmetry in the charge density, which is directed toward the lead sites above and below the plane and thus demonstrates the relationship of the trapped charge to the missing charge at the lead atoms.

The analysis described is significant not only because it conclusively demonstrates the existence of a new type of chemical bond, but also because it shows that centers with small scattering cross sections can be located accurately by x-ray diffraction techniques, provided that the full correction is made for anomalous dispersion.

P. M. Raccah
J. M. Longo
J. B. Goodenough

G. NÉEL TEMPERATURES IN PEROVSKITE AND RELATED STRUCTURES

It has been shown previously[13] that transition-metal oxides having the perovskite structure exhibit cationic d orbitals that may be either localized or collective, depending primarily upon the principal quantum number, the formal cationic charge, and the potential number of unpaired spins for localized electrons. Further, the transition from a localized-electron to a collective-electron state is sharp and apparently first-order.[17] In the perovskite structure, the transition-metal cations are in octahedral sites, so that the crystalline fields distinguish d orbitals of t_{2g} and e_g symmetry. Further, the d electrons on neighboring cations are coupled to one another via 180° cation-anion-cation superexchange, t_{2g} with t_{2g} and e_g with e_g. With one electron per interacting orbital, as on Cr^{3+} or $Mn^{4+}(t^3e^0)$ and $Fe^{3+}(t^3e^2)$, the interatomic-exchange correlations are antiferromagnetic, whether the electrons are localized or collective. If the d electrons are localized, it follows from superexchange and molecular-field theory that the antiferromagnetic Néel temperature is

$$kT_n \approx z\{q_t b_t^2 + q_e b_e^2\}\ (S + 1)/S \qquad (1)$$

where z = 6 is the number of near-neighbor cations in a cubic perovskite, q_t and q_e are inversely

proportional to electrostatic energies associated with t_{2g} and e_g electron transfers creating excited states, and $b_i \sim \epsilon_i \Delta_i$ are the one-electron transfer integrals. The atomic moments approach the spin-only moments $\mu_s = 2S\mu_B$. Since q_t and q_e both increase with increasing transfer integral, T_N increases sensitively with increasing b_t and/or b_e until a critical value b_c is reached. For $b > b_c$, the outer electrons are collective with bandwidths $\Delta\epsilon_\pi \sim b_c$ and $\Delta\epsilon_\sigma \sim b_e$. In the collective-electron state, T_N should decrease with increasing bandwidth, disappearing for $b > b_c^f$, where $b_c^f > b_c$ is sharply defined but sensitive to the number of electrons in the narrow d-bands. It follows that T_N should reach its maximum value for $b \approx b_c$. Since the overlap integrals Δ should increase with decreasing lattice parameter a_o, provided all else is kept constant, it follows that the variation of the Néel temperature with hydrostatic pressure should be

$$dT_N/dP > 0 \text{ for } b < b_c \tag{2}$$

$$dT_N/dP < 0 \text{ for } b > b_c \tag{3}$$

Studies have been made[18,19] on the perovskites $A^{3+}FeO_3$ and $A^{3+}CrO_3$ of the change in T_N with a_o, where the change in a_o was accomplished by chemical means rather than by hydrostatic pressure. It was found that T_N decreases with decreasing a_o for A = La, Y, or a rare-earth ion even though independent evidence indicates that the d electrons are localized in these compounds. What is the origin of this apparent contradiction of Eq. (2)? Although Treves et al.[20] have suggested this is due to a changing cation-anion-cation angle with changing lattice parameter, this would seem to give too small a contribution, so that some more general argument is required.

Now the crystalline orbitals of t_{2g} symmetry are

$$\Psi_t = N_\pi(f_t + \lambda_\pi \Phi_\pi) \tag{4}$$

where λ_π is the covalent mixing parameter, f_t is the cationic d orbital, and Φ_π represents the anion p orbitals that π-bond with the cation. Thus the overlap integral for t_{2g} orbitals is $\Delta_t \sim \lambda_\pi^2$. But these same anion p orbitals σ-bond with the large A cations, so that the stronger the σ-bond the smaller the competitive λ_π. Further, the larger the A cations, the more they are ionic, or the smaller the A-O σ-bonding. Hence λ_π increases with increasing a_o if this change is due to substitution of a larger A cation. Therefore the only adequate test of Eq. (2) is a pressure experiment.

MacChesney et al.[21] have tried to test Eq. (1) by varying the number of magnetic near-neighbors z. Whereas $KNiF_3$, with z = 6, has T_N = 275°K, and K_2NiF_4, with z = 4, has T_N = 180°K, nevertheless they found that in the series $CaMnO_3$, $Ca_4Mn_3O_{10}$, $Ca_3Mn_2O_7$, and Ca_2MnO_4, where z varies from 6 to 5-1/3 to 5 to 4, the Néel temperatures are T_N = 123°, 125°, (120°) and 114°K. In this case the large A cation is always Ca^{2+}, so that λ_π should depend primarily on a_o. Since there is a steady decrease in a_o with increasing Ca/Mn ration, this effect would tend to increase T_N as the decrease in z simultaneously tends to decrease T_N. If these two effects cancel each other, this could account for the results. However, there is another factor that appears to be playing an important role: the magnetic and electrical data suggest that $b \approx b_c$ for $Ca_3Mn_2O_7$, and this appears to be a more profound reason for the apparent maximum in T_N on going through this series.

J. B. Goodenough

REFERENCES

1. Solid State Research Report, Lincoln Laboratory, M.I.T. (1967:1), p.24, DDC 651065.
2. C.F. Guerci and M.W. Shafer, J. Appl. Phys. 37, 1406 (1966).
3. H.A. Eick, N.C. Baenziger, and L. Eyring, J. Am. Chem. Soc. 78, 5148 (1956).
4. B.B. Kosicki, W. Paul, A.J. Strauss, and G.W. Iseler, Phys. Rev. Letters 17, 1175 (1966).
5. Solid State Research Report, Lincoln Laboratory, M.I.T. (1966:4), p.31, DDC 647688.
6. G.E. Stillman, private communication.
7. Solid State Research Report, Lincoln Laboratory, M.I.T. (1966:4), p.24, DDC 647688.
8. W.A. Bassett, T. Takahashi, and P.W. Stock, Rev.Sci. Instr. 38, 37 (1967).
9. L.H. Adams and B.L. Davis, Amer. J. Sci. 263, 363 (1965).
10. S. Andersson, B. Collen, U. Kiylenstierna, and A. Magneli, Acta Chem. Scand. 11, 1641 (1957).
11. S.P. Denker, J. Phys. Chem. Solids 25, 1397 (1964).
12. J.K. Hulm, C.K. Jones, R. Mazelsky, and R.C. Miller, Bull. Am. Phys. Soc. 10, 44 (1965).
13. J. B. Goodenough, J. Appl. Phys. Suppl. 37, 1415 (1966), DDC 640998.
14. Solid State Research Report, Lincoln Laboratory, M.I.T. (1966:3), p.20, DDC 641498.
15. M. Tokonami, Acta Cryst. 19, 486 (1965).
16. D.T. Cromer and J.T. Waber, Acta Cryst. 18, 104 (1965).
17. P.M. Raccah and J.B. Goodenough, Phys. Rev. 155, 932 (1967).
18. J.B. Goodenough, Landolt-Bornstein Tabellen, Vol.II, Part 9, p.2-208 (1962).
19. R. Aléonard, R. Pauthenet, J.P. Reboillat, and V. Zarubica, Compt. Rend. 262, 866 (1966).
20. D. Treves, M. Eibshütz, and P. Coppens, Phys. Letters 18, 216 (1965).
21. J.B. MacChesney, H.T. Williams, J.F. Potter, and R.C. Sherwood, private communication.

IV. PHYSICS OF SOLIDS

A. ELECTRONIC BAND STRUCTURE

1. Magneto-electroreflectance at Liquid Helium Temperatures*

In earlier work the power of electric field modulation of the magnetoreflection was demonstrated by using the electrolyte method at room temperature. Unfortunately this technique cannot be extended to liquid nitrogen or helium temperatures because the electrolyte freezes, or to wavelengths longer than 2 μ because of absorption by the electrolyte. A mechanically integrated thin film package has been developed† which eliminates these two restrictions. The package is fabricated by first coating the etched sample surface with an insulating layer (~1 μ thick) of photoresist and then evaporating a thin nickel or inconel film (<100 Å thick) on the photoresist as the transparent electrode. With this arrangement it is possible to apply electric fields of the order of 5×10^5 V/cm to a sample which is cooled to pumped liquid helium temperatures (~1.5°K), and to take measurements at wavelengths in the infrared, at least out to 20 μ.

So far, magneto-electroreflection results have been obtained in germanium, InSb, InAs and HgTe. Spin-orbit split valence band to conduction band transitions have been observed in germanium, InSb and, for the first time, in InAs.

The sensitivity of this technique seems comparable with that of the piezoreflectance; electroreflectance has the advantage over piezoreflectance of permitting lower working temperatures without stressing the sample, but the disadvantage of losing some light through the transparent electrode.

S. H. Groves
C. R. Pidgeon‡
J. Feinleib

2. Study of Exciton Fine Structure in the Interband Magnetoabsorption of InSb and Germanium

In our study of exciton fine structure in InSb[1,§] extra absorption lines were observed which could not be explained by the theory of Elliott and Loudon.[2] We have recently examined the lowest absorption peaks in the interband magnetoabsorption spectrum of germanium. As in InSb, a strong symmetrical absorption peak is observed followed, at higher energies, by an absorption edge with the absorption tailing off slowly toward higher energies. These features correspond to the formation of an exciton in the ground state and in the quasi-continuum of excited exciton states, respectively. However, anomalous peaks, such as those seen in InSb, were not observed in germanium. This suggests that the anomalous exciton peaks of InSb correspond to a forbidden transition that is turned on because of the lack of inversion symmetry in InSb. Indeed, Bell and

* Part of this work was carried out using the high field facilities of the National Magnet Laboratory, M.I.T.
† It is a pleasure to acknowledge many helpful suggestions by T. Herndon of Group 23.
‡ National Magnet Laboratory, M.I.T.
§ An unpublished work by the author.

Rodgers[3] have predicted this effect with intensities and energy separations, relative to the allowed transitions, which compare favorably with the observed anomalous exciton peaks.

A quantitative theoretical analysis of the exciton in a high magnetic field in InSb or germanium is complicated by the nature of their valence bands and by central cell effects. Calculations for InSb in a magnetic field using values of hole mass ranging from that of the heavy hole to infinity, yield exciton binding energies that are from 10 to 15 percent below the experimental values. This suggests that the precise choice of hole mass is not important and that central cell effects are significant.

E. J. Johnson

3. Magneto-Optical Investigation in BiSb Alloys

Oscillations in the magnetoreflection of $Bi_{0.97}Sb_{0.03}$* have been observed using the apparatus previously described by Brown and co-workers in their work on pure bismuth.[4] Magnetoreflection oscillations obtained from a binary face with the magnetic field along the binary axis

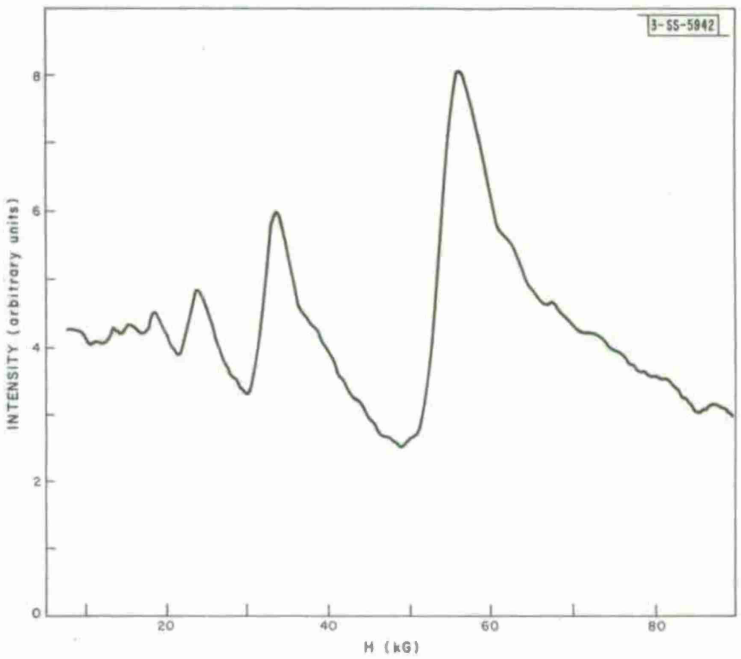

Fig. IV-1. Oscillations in magnetoreflection from binary face of $Bi_{0.97}Sb_{0.03}$. Magnetic field is along a binary axis.

are shown in Fig. IV-1. These oscillations are quite sharp and are identified with interband transitions between the Landau levels of the strongly coupled bands. The data is being interpreted in terms of the Lax two-band model for the non-parabolic tilted ellipsoidal energy surfaces. This investigation is being undertaken to determine energy band changes in the transition from semimetal to semiconductor as bismuth is alloyed with small amounts of antimony.

E. J. Tichovolsky†
D. F. Kolesar

* This alloy was kindly prepared by Dr. K. F. Cuff of the Lockheed Palo Alto Research Laboratory.
† Department of Physics, M.I.T.

4. Analysis of Current Modulated Reflectance of Gold

Previously reported measurements of the current modulated reflectance of gold[5] exhibited important structure in the region from 2.4 to 2.6 eV, where a sharp drop in the reflectivity occurs due to the onset of interband transitions. In this report, we present a brief account of our attempts to analyze this structure.

Ehrenreich and his co-workers[6] have considered the onset of interband transitions in the noble metals and have calculated the joint density of states, ρ, for direct interband transitions between a lower d band and an upper conduction band. ρ is given by the expression

$$\rho_{d\text{-cond}} = \frac{2}{(2\pi)^3} \int d\vec{k}(F_d - F_c)\, \delta(\omega_{d-c} - \omega) \tag{1}$$

where F_d and F_c are the Fermi distribution functions for the d and conduction bands respectively. Since the imaginary part of the dielectric constant, ϵ_2, and its increment, $\Delta\epsilon_2$, can be obtained from the optical measurements, let us consider the theoretical ϵ_2 at the onset of interband transitions which is given by

$$\epsilon_2 \simeq \frac{e^2\hbar}{2\pi m} \frac{1}{(\hbar\omega)^2} \int \frac{2}{m} |p^{\mu}_{d-c}|^2 (F_d - F_c)\, \delta(\omega_{d-c} - \omega)\, d\vec{k} \tag{2}$$

where $2/m\, |p^{\mu}_{d-c}|^2$ is the momentum matrix element between the states. In the small region of k-space in which we are interested we may consider $2/m\, |p^{\mu}_{d-c}|^2$ as constant; then

$$\epsilon_2 = \frac{2\pi^2 e^2 \hbar}{m} \frac{1}{(\hbar\omega)^2} \frac{2}{m} |p^{\mu}_{d-c}|^2\, \rho \tag{3}$$

Therefore, if we know the magnitude of such quantities as $2/m\, |p^{\mu}_{d-c}|^2$ and the variation of ρ with our modulating parameter we can compare a calculated $\Delta\epsilon_2$ with our measured $\Delta\epsilon_2$.

In the current modulation technique, $\Delta\rho$ arises from temperature-induced strain effects as well as explicit temperature effects. The strain effects have the important result of shifting the Fermi level and changing the level spacings. Neglecting effects such as modulation electron-phonon interactions which are probably small, we may write

$$\Delta\rho = \frac{\partial\rho}{\partial T} \Delta T + \frac{\partial\rho}{\partial E_{d-F}} \Delta E_{d-F} \tag{4}$$

where E_{d-F} is the separation between the d-band and conduction band at the Fermi level.

From pressure experiments,[7] the variation of E_{d-F} with strain is known. The momentum matrix element $2/m\, |p^{\mu}_{d-c}|^2$ is approximately known. Without going into detail, an analysis of the piezoreflection data on gold,[8] in which the first term in Eq. (4) does not enter, indicates that the values of $2/m\, |p^{\mu}_{d-c}|^2$ usually quoted[2,9] are too small by a factor of 2 to 4 to account for the experimentally deduced $\Delta\epsilon_2$. However, the qualitative features of the piezoreflectance results near 2.5 eV are consistent with the analysis. In the current or temperature-modulated case, the line shape of $\Delta\epsilon_2$ around 2.5 eV is different but again the analysis qualitatively predicts the line shape. ΔT is unknown but we can assume ΔE_{d-F} is proportional to ΔT. Knowing $\partial\rho/\partial T$ from the Fermi distribution function, we find that if only dilatation is considered in the

calculation of $\partial\rho/\partial E_{d-F}$, a ΔT of about 25° is necessary to account for our results. This seems unreasonable; it appears that shear effects, which are quantitatively unknown, should be included in the analysis.

Although a quantitative analysis may be difficult, the qualitative agreement with observed structure in gold gives us confidence that with these techniques we can obtain useful information concerning the bands involved in the onset of interband transitions. This seems to be particularly important for nickel, where analysis of recent data[10] now being conducted indicates that we may be able to resolve the question of the correct band model for this substance at the L point (111) in the Brillouin zone.

J. Hanus
W. J. Scouler

5. Donor Impurity Levels for InSb in a Magnetic Field

Recent experimental investigations of the energy levels of donor impurity atoms in InSb in a magnetic field have prompted the present attempt to calculate the impurity atom ground state and the lowest lying $M = \pm 1$ excited states.

Calculating in the effective mass approximation, we use the 8×8 matrix Hamiltonian of Bowers and Yafet[11] to describe the conduction electron in the external magnetic field; we add to this the matrix $-(e^2/\epsilon_o r)\,\delta_{ij}$ to account for the Coulomb attraction of the donor. The resulting matrix can, to a good approximation, be reduced to a single Schrodinger equation, whose conduction band eigenvalues were calculated by a variational method. The trial envelope functions used, containing four variational parameters, were quite flexible: when applied to the hydrogen atom in a magnetic field in a simple parabolic band, we obtained energies over a wide range of magnetic field strengths for both $M = 0$ and $M = \pm 1$ states which are lower than previously published values.

Comparison of our results with the experiments of R. Kaplan[12] and D. Dickey,* suggests that a central cell correction which increases with magnetic field, must be applied to the energy of the ground state to bring theory and experiment into quantitative agreement. This conclusion is, however, only tentative, pending further experimental testing.

D. M. Larsen

6. Phonon Dispersion Relations for Silicon and Germanium

The application of the Fourier expansion technique to obtain the phonon dispersion relations has been discussed in the preceding Solid State Research Report.† In that work, the band parameters of Fourier expansion coefficients for silicon and germanium were evaluated using experimental measurements of the elastic constants and of the vibrational spectrum as obtained by neutron diffraction.

Within the framework of the force constant model of the Born-von Karman theory, the Fourier expansion is relatively slowly convergent. To improve the convergence, a shell model for the lattice vibrations has been introduced.

---

* Unpublished.

† Solid State Research Report, Lincoln Laboratory, M.I.T. (1967:1), DDC 651065.

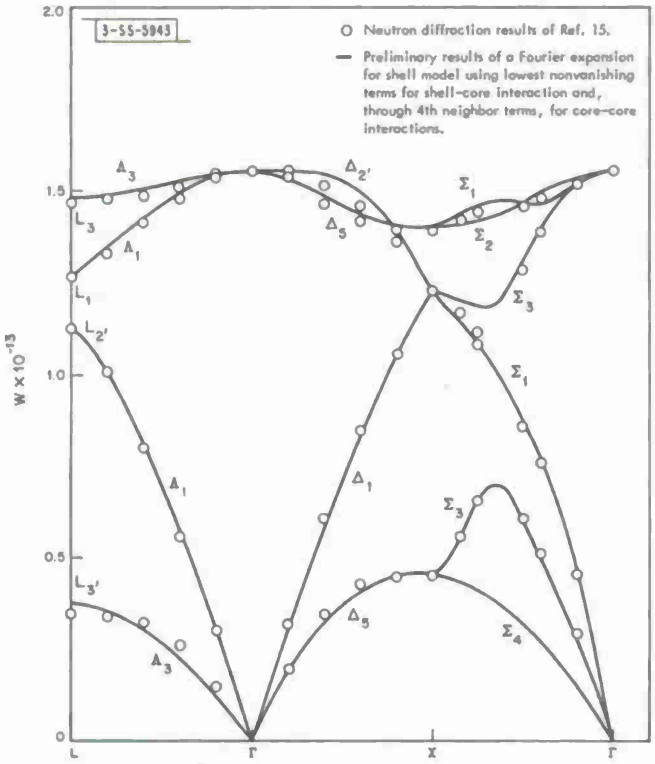

Fig. IV-2. Phonon dispersion relations for Si.

The shell model, suggested by Dick and Overhauser,[13] and applied by Cochran[14] and Dolling[15] to the diamond structure, has been formulated using the Fourier expansion technique. By allowing the atoms to deform, two coordinates for each atom are introduced and the dimensionality of the problem is doubled. The coupling of the shells to each other and to their ion cores is handled in terms of coupled systems, in a manner completely analogous to the coupled s and p bands of the electron problem. The more rapid convergence of the Fourier expansion for the coupled problem is illustrated in Fig. IV-2. In this figure, the experimental neutron data for silicon[15] is compared with the calculated values using up to and including fourth nearest neighbor terms for the ion cores and the lowest nonvanishing terms for the core-shell interaction.

G. Dresselhaus
Mildred S. Dresselhaus

B. TRANSPORT PHENOMENA

1. Transport Anomalies in Ti_2O_3

Our earlier work on Ti_2O_3[16,17] has indicated the absence of magnetic order at low temperatures. However, a transition to a magnetically ordered state has been offered by other workers[18,19] as an explanation for the sharp increase in resistivity with falling temperature in the neighborhood of 540°K. This theory is in conflict with our magnetoresistance results, and its predictions depart from the experimental resistivity behavior in some important details.

We have considered some simple models of possible band structures for Ti_2O_3 and calculated resistivities from them. The observed magnetoresistance effects make it imperative to use at least a two-band model. The crystal parameters, and in particular, the ratio c/a, vary strongly as functions of temperature in the same range as the resistivity variation.[20] In our models, therefore, we assumed that the energy band structure would also change in the "transition region." We adjusted the parameters of the models to see what sort of energy band restructuring was required to explain the observed resistivity changes. We found that a continuous variation of either conduction band width or of valence band to conduction band separation can produce resistivities agreeing with the experiments in all important respects (Fig. IV-3). It proves necessary to allow the two bands partially to overlap at high temperatures.

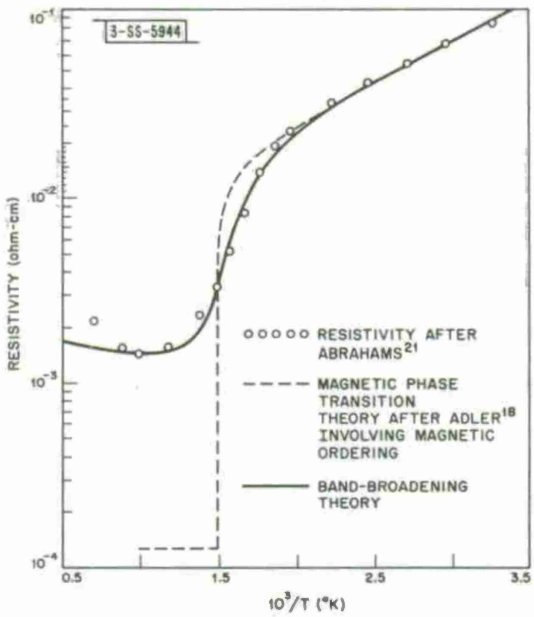

Fig. IV-3. Plot of log ρ vs 1/T for single crystal Ti_2O_3.

In the band-broadening model, the conduction band approximately doubles in width. In the band-shifting model, a relative shift of 0.2 or 0.3 electron volt is required. The crystallographic changes are sufficiently great that neither of these possibilities seems unreasonable.

We have also studied the Hall coefficient and the thermoelectric power. Anomalous behavior of the latter in the transition region offers a way of checking experimentally some features of the band-broadening model.

L. L. Van Zandt
J. M. Honig

2. Quasi-Particle Transport Equation of a Fermi Liquid in the Presence of Dilute Random Impurities

Recently a derivation of the Landau transport equation has been given for a system of fermions in the presence of dilute static impurities.[22] This work was carried through by the use of zero temperature perturbation theory (real-time diagram techniques). It is well known that the applicability of the zero temperature techniques is limited. The use of such a method is not always justified in a nonuniform system. Furthermore, it is clear that in the zero temperature formulation one is forced to use the perturbation technique holding the number of particles

fixed and not the chemical potential. In the impurity problem this leads one to conclude that a chemical potential cannot be defined unambiguously.

We have attacked this problem using the temperature technique developed by Luttinger and Ward.[23] This method has several advantages:

(a) Its applicability is not in doubt in nonuniform systems; it is therefore suited to the impurity problem.

(b) The chemical potential can be defined unambiguously, since in the temperature technique it is possible to hold the chemical potential fixed when doing perturbation theory. These facts allow us to remove some of the ambiguities found in the method of Ref. 22.

(c) The technique is designed to be used at nonzero temperatures. We have carried out our calculation only in the limit of zero temperatures. We feel that it is possible to obtain the first temperature corrections from this method.

We have so far derived the same equation as found in Ref. 22, which is accurate to zeroth order in the parameters $q \cdot v$, ω, Γ and neglects terms of second order and higher in the density of impurities as well as all terms of order $q \cdot v/\mu$, ω/μ, Γ/μ and higher; here q is the wave-vector of the disturbance, v, the quasi-particle velocity, Γ, the lifetime due to impurities and μ, the chemical potential.

J. L. Sigel
P. N. Argyres

C. MAGNETISM

1. Neutron Diffraction Study of $ZnCr_2S_4$

A neutron diffraction investigation of $ZnCr_2S_4$ has been undertaken in order to provide greater insight into the distant-neighbor magnetic interactions[24] in spinels with nonmagnetic A-sites. The diffraction pattern at 77°K established that this material is a normal spinel (i.e., that the zinc ions are located on the tetrahedral A-sites, the chromium ions are on the octahedral B-sites) and the oxygen parameter is 0.3835 ± 0.0005. On reducing the temperature below the Néel value,[25] T_N = 18°K, a spiral pattern with a wave vector along the (00ℓ) direction is found. However, as the temperature is further reduced a more complicated diffraction pattern occurs, involving additional wave vectors. At the same time, there appears to be a slight reduction in the intensities of the peaks corresponding to the original (00ℓ) vector.

A thorough study of the magnetic behavior of the material requires considerable auxiliary equipment which is available at the Brookhaven National Laboratory. We have therefore initiated a collaborative study with Dr. L. Corliss and Dr. J. Hastings of that laboratory.

N. Menyuk
K. Dwight
A. Wold*

2. Antiferromagnetic Resonance in the Insulating Magnetic Spiral Structure MnI_2

Antiferromagnetic resonance has been observed in single crystals of MnI_2 at liquid helium temperatures and in the range of frequencies from 35 to 70 GHz. Neutron diffraction studies[26]

* Brown University, Providence, Rhode Island.

have shown that the Mn^{2+} spins order in a flat spiral spin configuration below 3.48°K and with a spin propagation vector along the [307] direction. The resonance data indicates the presence of appreciable short range ordering at 4.2°K. At the lowest temperature reached by pumping on liquid helium, namely ~1.5°K, the sample had a zero-field resonance at 48 GHz. At this temperature the resonance frequency varied almost quadratically with applied fields. Several weaker resonances were also observed at the lower temperatures; the origin of these lines is as yet uncertain. All the resonances exhibit some anisotropy with applied field which could be attributed to demagnetizing effects in the planar sample. We are attempting a theoretical analysis of the resonance based on a modification of the calculations of Cooper et al.[27]

J. J. Stickler
H. J. Zeiger

3. High-Temperature Expansions for the Classical Heisenberg Model – Energy, Entropy and Specific Heat

The following is an abstract of a paper scheduled to appear in Phys. Rev.[28]

"The high-temperature series expansion of the zero-field magnetic susceptibility, $\chi/\chi_{Curie} = 1 + \Sigma_{\ell=1}^{\infty} a_\ell (J/kT)^\ell$, is related to the diagrammatic representation of the corresponding high-temperature expansion of the zero-field static spin correlation function $\langle S_f \cdot S_g \rangle_\beta$ presented in paper I.[29] The first nine terms a_ℓ for loose-packed lattices and the first seven terms for close-packed lattices in the susceptibility series are explicitly obtained in terms of Domb's 'general lattice constants' $p_{\ell x}$. The general lattice expressions are then used to evaluate these a_ℓ numerically for three two-dimensional lattices and for three cubic lattices. Finally, the a_ℓ are employed to discuss two questions of current interest: (i) Does the critical exponent γ – in the assumed form of the divergence of χ, $\chi \sim (T - T_c)^{-\gamma}$ as $T \to T_c^+$ – have the value 4/3 for the fcc, bcc, and s.c. lattices? (ii) Do high-temperature expansions suggest a phase transition ($T_c \neq 0$) for some two-dimensional lattices with nearest-neighbor ferromagnetic interactions? It is argued that extrapolation suggests γ is definitely greater than 4/3 for the fcc, bcc, and s.c. lattices, and that T_c is appreciably different from zero for the plane square and triangular lattices."

H. E. Stanley

4. High-Temperature Expansions for the Classical Heisenberg Model – Zero-Field Susceptibility

The internal energy, entropy and specific heat may be simply related to the partition function $Z \equiv \text{trace}\, e^{-\beta \mathcal{H}}$ of any magnetic system. In fact, the same coefficients λ_n enter in the high-temperature expansions for all three functions. These coefficients λ_n are just the cumulants of the Hamiltonian, and are defined by the expression

$$\frac{1}{N} \log Z = \log(2S + 1) + \sum_{n=2}^{\infty} \lambda_n \frac{K^n}{n!} \tag{5}$$

where $K \equiv 2J/kT$, and $2J$ is the nearest-neighbor exchange interaction. Hence the internal energy (per spin) $E \equiv \langle \mathcal{H} \rangle_T \equiv -2J(\partial/\partial K) \log Z$ is given by

$$E = -2J \sum_{n=2}^{\infty} \lambda_n \frac{K^{n-1}}{(n-1)!} \tag{6}$$

Similarly, the specific heat $C \equiv \partial E/\partial T$ may be expanded as

$$C = k \sum_{n=2}^{\infty} \lambda_n \frac{K^n}{(n-2)!} \tag{7}$$

where k is Boltzmann's constant. Finally, the entropy S may be obtained directly from E and $F \equiv -kT \log Z = E - TS$.

It is our purpose here to present the results of a calculation of the first ten coefficients λ_n for loose-packed lattices and the first nine λ_n for close-packed lattices. This calculation exploits the order-of-magnitude simplifications which occur[30] in treating the quantum-mechanical spin operators in the Heisenberg model as classical vectors of length $[S(S+1)]^{1/2}$. The coefficients λ_n were obtained by two independent methods: (a) from a recursion relation[31] involving the moments $\mu_n \equiv \langle \mathcal{H}^n \rangle$ of the Heisenberg Hamiltonian $\mathcal{H} = -\Sigma_{ij} J(i,j) \vec{S}_i \cdot \vec{S}_j$, and (b) from the diagrammatic representation of the nearest-neighbor spin correlation function.[29] We first obtain expressions for the coefficients λ_n in terms of general lattice constants[32] (Table I); we then evaluate the λ_n numerically for three two-dimensional lattices and three cubic lattices (Table II).

H. E. Stanley

5. Similarity Between S = 1/2 Ising and S = ∞ Heisenberg Models

Oguchi[33] developed the zero-field reduced susceptibility $\bar{\chi}^I = \chi^I/\chi^I_{Curie}$ of the $S = 1/2$ Ising model as a power series in the variable $v = \tanh K$, where $K \equiv 2J/kT$, and J is the nearest-neighbor exchange parameter. This suggests we seek an expansion parameter more natural than K for the reduced susceptibility $\bar{\chi}^H$ of the classical ($S = \infty$) Heisenberg model.

Using the results of a previous publication[28] (see also Sec. IV-C-3 of this report), we have obtained general-lattice expressions through order u^9 (u^8 for close-packed lattices) for the coefficients A_j in the expansion

$$\bar{\chi}^H = 1 + \sum_{n=1}^{\infty} A_n u^n \tag{8}$$

where the new expansion parameter u is the Langevin function $\mathcal{L}(K) = \coth K - 1/K$. In addition, we have made the following observations:

(a) The radii of convergence $u_c = \mathcal{L}(K_c)$ of Eq. (8) estimated by standard extrapolation procedures, agree with the radii of convergence K_c of the conventional expansion

$$\bar{\chi}^H = 1 + \sum_{n=1}^{\infty} a_n K^n \tag{9}$$

TABLE I

GENERAL-LATTICE EXPRESSIONS FOR THE COEFFICIENTS λ_n

(Notation is as used in Ref. 32)

$$\lambda_2 = z/6$$

$$\lambda_3 = (2/3)\, p_3$$

$$\lambda_4 = (8/45)\,(5p_4 - 3z/8)$$

$$\lambda_5 = (8/27)\,(5p_5 - 9p_3)$$

$$\lambda_6 = (16/27)\,(5p_6 - 12p_4 - 9p_{5a} - 5.7p_3 + 3z/14)$$

$$\lambda_7 = (112/81)\,(5p_7 - 15p_5 - 9p_{6b} - 18p_{7g} - 114p_{5a}/5 + 459p_3/35)$$

$$\lambda_8 = (896/243)\,(5p_8 - 18p_{8r} - 18p_{8s} - 114p_{7c}/5 - 9p_{7b} - 9p_{7a} - 1071p_{6d}/25 - 57p_{6b}/5 - 171p_{6a}/5 - 18p_6 + 1206p_{5a}/35 + 5133p_4/350 + 783p_3/35 - 81z/560)$$

$$\lambda_9 = (896/27)\,(5p_9/3 - 6\,[p_{9h} + p_{9f} + p_{9e}] - [38/5]\,[2p_{9g} + p_{8p} + p_{8e}] - 3p_{8b} - 3p_{8a} - 238/25\,[p_{8q} + p_{7h}] + 1356p_{7g}/35 - 19/5\,[2p_{7f} + p_{7b}] - 7p_7 + 27p_{7c}/5 + 1576p_{6b}/175 + 8556p_{5a}/175 + 72p_5/7 - 611p_3/245 + 1272p_{6d}/25)$$

$$\lambda_{10} = (8960/81)\,(5p_{10}/3 - 6\,[p_{10b} + p_{10c}] - 3p_{9k} - 238p_{8t}/25 + 144p_{8r}/5 - 38p_{8c}/5 - 8p_8 - 38p_{9m}/5 + 1142p_{7a}/175 + 10008p_{6a}/175 + 99p_6/7 + 12p_4/175 + 27z/770)$$

TABLE IV-2

THE ZERO-FIELD FREE ENERGY COEFFICIENTS λ_n

n	Honeycomb	Square	Triangular	Simple Cubic	Body-Centered Cubic	Face-Centered Cubic
2	0.5000	0.6667	1.0000	1.0000	1.3333	2.0000
3	0	0	1.3333	0	0	5.3333
4	−0.1333	−0.2000	2.2667	2.2667	10.1333	28.5333
5	0	0	3.5556	0	0	227.5556
6	1.8624	−0.6772	1.1175	44.6138	354.2011	2,421.9090
7	0	0	−41.7185	0	0	32,792.6519
8	−34.7852	−18.1149	−425.3472	1,917.8430	33,179.4015	543,302.6212
9	0	0	−3,703.3764	0	0	10,665,327.4841
10	793.8586	−418.9474		173,295.4505	6,169,985.0056	

for all three-dimensional and for all two-dimensional lattices studied. For the one-dimensional lattice (linear chain), the coefficients a_n behave so irregularly with n that the radius of convergence cannot be estimated by extrapolation. However, the coefficients A_n do behave smoothly for the linear chain, and indeed predict the known[34] value for the radius of convergence, $u_c = 1$ ($K_c = \infty$, or $T_c = 0$).

(b) It is well known that in the Bethe-Peierls approximation[35,36]

$$\bar{\chi}^I = \frac{1+v}{1-\sigma v} \quad , \quad \bar{\chi}^H = \frac{1+u}{1-\sigma u} \tag{10}$$

where $\sigma \equiv z - 1$, and z is the lattice coordination number. This suggests the following expansions of the exact Ising*[37] and Heisenberg models

$$\bar{\chi}^I = (1-\sigma v)^{-2}\left[1 - (\sigma - 1)\, v - \sigma v^2 + \sum_{n=3}^{\infty} D_n^I v^n\right] \tag{11}$$

and

$$\bar{\chi}^H = (1-\sigma u)^{-2}\left[1 - (\sigma - 1)\, u - \sigma u^2 + \sum_{n=3}^{\infty} D_n^H u^n\right] \tag{12}$$

It is straightforward, albeit somewhat tedious, to calculate the coefficients D_n in terms of the basic lattice constants p_{nx}. Whereas the A_n were quite complicated functions of the p_{nx} (involving each p_{nx} multiplied by a complicated nth order polynomial in σ), the new coefficients D_n are quite simple and are independent of σ, e.g., $D_3^I = D_3^H = -6\, p_3$ and $D_4^I = -8\, p_4 = D_4^H + (24/5)\, p_3$.

H. E. Stanley

*M. F. Sykes has carried out the expansion (Eq. 11) for the Ising model.

D. SCATTERING EXPERIMENTS WITH LASERS

1. Raman Scattering from Donor and Acceptor Impurities in Silicon

We have observed electronic Raman scattering from phosphorous donor and boron acceptor impurities in silicon. We find that the most important intermediate states involve interband transitions, and that this has important consequences for the intensity of the scattering. The results of the acceptor scattering experiment will be of great use in the future extension of theoretical impurity calculations. We have also observed phonon Raman scattering involving the creation of one virtual zone-center optical phonon with subsequent decay through the anharmonic interaction into two acoustic phonons. A more detailed description has been published.[38]

G. B. Wright
A. Mooradian

2. Anomalous Microwave Absorption and Emission of Interstellar OH

The ultraviolet-pumping model[39] for interstellar 18-cm OH emission and anomalous absorption has been extended to include the effects of thermal electron collisions, varying amounts of overlap of the Doppler-broadened ultraviolet hyperfine-split absorption lines, and selective far-infrared absorption. In the presence of strong electron collision rates, far-infrared or ultraviolet continuum pumping and selective absorption can produce, respectively, 1612 or 1720 MHz emission, with the remaining three transitions becoming anomalously absorbing.* For weaker electron collision rates and for kinetic temperatures high enough to cause overlap of the hyperfine-split ultraviolet pump absorption lines, all four hyperfine transitions are inverted over the same region in the OH cloud; but for cooler clouds, the inversion regions for the different transitions become separated, especially for 1667 and 1665 MHz. Similar calculations on SH indicate that Λ-doublet population inversion is also possible for this species.

For relatively slow thermalization of OH molecular velocities and for propagation nearly parallel to the pump, the ultraviolet selective absorption produces an unsaturated gain-frequency profile, which may be narrower than the Doppler width and which may have a dip at line center. A stability analysis for pure circular polarization is considered for cases of saturated broad band maser emission between states with Zeeman frequency splittings which are larger than the inverse lifetimes of the states.† The analysis involves Raman-type cross-saturation, combination-tone generation and magnetoplasma propagation.

M. M. Litvak M. L. Meeks
A. L. McWhorter H. J. Zeiger

3. Mode Structure in a Resonant Raman Oscillator

The splitting of the 467 cm^{-1} Stokes lines into two or three sharp components which has been observed in stimulated Raman scattering in quartz at low temperatures can be explained plausibly on the basis of quartz resonator mode splitting and mode pulling. A number of samples were

---

* This is similar to the data of W. M. Goss.[40]

† This is contrary to the cases considered by Heer and Bender.[41]

used ranging in length from 0.6 to 2.2 cm, each in the form of a cavity with plane, parallel end faces. The Raman Stokes splittings, which were measured with an etalon, correspond nearly to the Fabry-Perot resonant modes of the quartz samples. However, the modes are consistently spaced 20 percent closer than expected from the cavity lengths. It would be surprising if such a large effect could be explained simply on the basis of a nonlinear index of refraction. The quartz samples are relatively low Q, high gain Raman oscillators because (a) the uncoated end walls are very lossy, and (b) Raman threshold can be reached even without parallel end faces. Because the spontaneous Raman line narrows to within an order of magnitude of the quartz cavity linewidth at low temperatures, mode pulling could possibly account for the magnitude of the observed splittings.*

Consider an optical cavity resonator filled with an active medium which can be pumped so as to exhibit population inversion. It is well known that when the atomic resonance ν_a of a dispersive medium in a Fabry-Perot resonator does not coincide with the cavity resonance ν_c, the cavity resonance will be pulled toward the atomic line center. This phenomenon, known as mode pulling, is described by†

$$\nu \cong \nu_c + (\nu_a - \nu_c) \frac{\Delta\nu_c}{\Delta\nu_a} \tag{13}$$

where ν is now the actual oscillating frequency, and $\Delta\nu_c$ and $\Delta\nu_a$ are the cavity and atomic linewidths, respectively. Hence the mode spacing between two oscillating cavity modes (ν'_c and ν_c) is given by

$$\nu' - \nu = (\nu'_c - \nu_c) \left(1 - \frac{\Delta\nu_c}{\Delta\nu_a}\right) \tag{14}$$

In our case the passive mode spacing is the usual Fabry-Perot frequency separation, $\nu'_c - \nu_c = 1/2nL$, where n is the refractive index of the cavity medium and L the cavity length. Thus the observed frequency splitting is

$$\Delta\nu = \frac{1}{2nL} \left(1 - \frac{\Delta\nu_c}{\Delta\nu_a}\right) \tag{15}$$

From Fig. IV-4, where $\Delta\nu$ is plotted vs $1/L$ for several discrete cavity lengths, the slope is 8.0, and thus $\Delta\nu_c/\Delta\nu_a = 0.17$. (The line of slope 9.7, drawn for comparison, represents the Fabry-Perot modes of a passive cavity with refractive index of 1.55.) Since the mode pulling data falls nearly on a straight line, $\Delta\nu_c/\Delta\nu_a$ must be almost constant. The spontaneous Raman linewidth‡ at 15°K is $\Delta\nu_a \cong 2.0 \pm 0.6\ \mathrm{cm}^{-1}$ (it is $6.6\ \mathrm{cm}^{-1}$ at 300°K and $3.1\ \mathrm{cm}^{-1}$ at 85°K); this would require a cavity width $\Delta\nu_c = 0.17 \times 2\ \mathrm{cm}^{-1} = 0.34\ \mathrm{cm}^{-1}$. In the simplified case when only end surface transmission contributes to cavity losses, the cavity frequency width is expressed

* This possibility was mentioned by Professor R. Y. Chiao.

† See, for example, W. R. Bennett, Jr., Appl. Opt. Suppl. on Optical Masers, p. 55 (1962).

‡ Measurement kindly performed by N. S. Strahm with a 50-mW He-Ne laser and a Spex double monochromator.

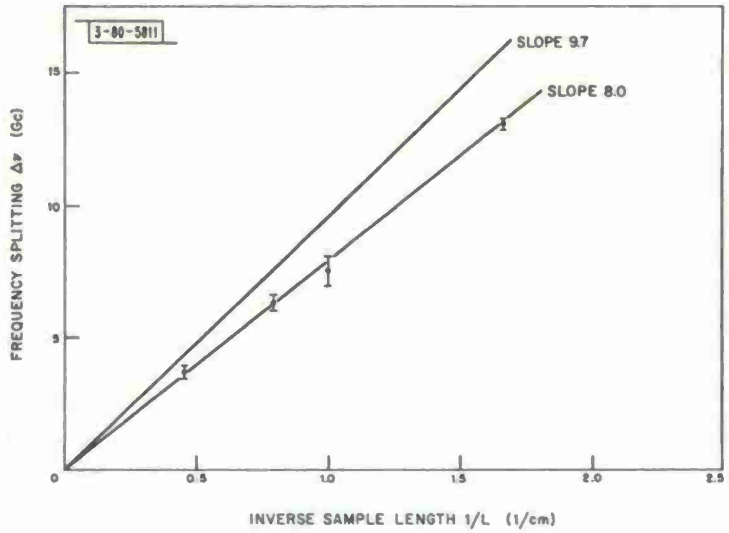

Fig. IV-4. Quartz Raman oscillator mode splitting as a function of inverse sample length at ~15°K.

by $\Delta\nu_c = f/2\pi nL$, where f is the fractional transmission; so for a 1-cm long sample $\Delta\nu_c \cong 0.1\ cm^{-1}$. Thus the numbers are of the correct order of magnitude. However, the fact that $\Delta\nu_c$ is almost independent of 1/L (as indicated by the constant slope fit) implies that another cavity loss factor must exist which is roughly proportional to L, perhaps related to the focusing geometry.

Qualitative evidence in support of the mode pulling explanation is the following:

(a) When the end surface of the quartz sample was coated with a reflecting film so as to raise the cavity Q, the modes approached the normal Fabry-Perot value.

(b) When three modes were observable, the intensity profiles showed that the weaker lines (which are displaced farther from the line center) were pulled the most.

(c) At higher power levels the mode pulling decreased, which is the same behavior as the "mode pushing" observed in gas lasers above threshold near line center.

(d) In a few cases where threshold could be reached at 120°K, the observed mode separation was nearer normal. There $\Delta\nu_a \cong 4\ cm^{-1}$, and the pulling factor $\Delta\nu_c/\Delta\nu_a$ is correspondingly diminished

(e) The simultaneously observed Brillouin shifts are normal.

(f) The second Stokes line is occasionally also seen to be split into components that show the same type of behavior described above for the first Stokes line.

G. S. Melanson, Jr. developed the SDS930 computer program which greatly facilitated the data reduction of the Fabry-Perot etalon measurements.

P. E. Tannenwald
F. H. Perry

4. Wide Range Continuously-Tunable High Power Sum Frequency Generation

A technique for producing high power, coherent light pulses whose frequency is continuously tunable over a 1000 Å range has been developed. The method is as follows: The output of a Nd glass laser is sent through a liquid cell (for example, CS_2 or chloronaphthalene) from which a broad band of frequencies results; then this broad band of frequencies is fed into a rotatable KDP crystal, as shown in Fig. IV-5. At the phase matching angle for second harmonic generation (SHG) of the Nd laser, radiation only at 5298 Å is observed, while on either side of this angle, two additional lines are observed, one below the second harmonic frequency with a power output of about 1 kW, and one above the second harmonic frequency with an output of about 10 W; phase matching here corresponds to using one ordinary ray plus one extraordinary ray added to produce one extraordinary ray.

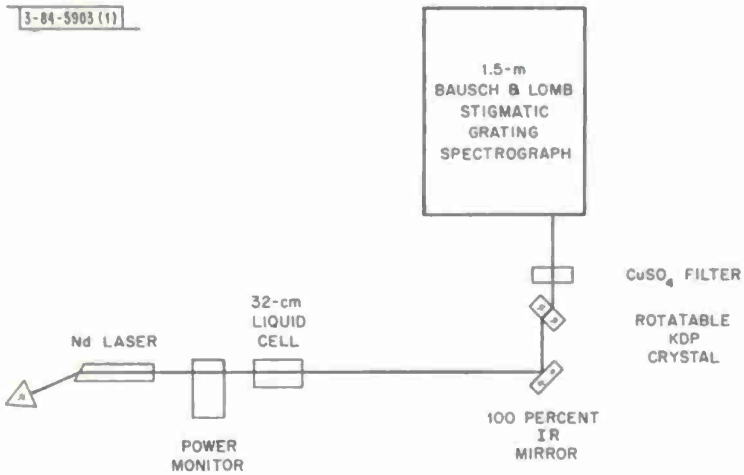

Fig. IV-5. Schematic of experimental apparatus for continuously tunable source.

The process causing the generation of these additional lines or side bands is phase-matched sum frequency generation in the KDP crystal, where one of the input frequencies is that of the Nd laser while the other is from among the nearly continuous output spectrum of the liquid cell. This near continuum is a manifestation of self-focusing and small scale trapping which occurs in the liquid cell when the laser power is high enough. The laser light gets trapped into filaments whose diameter is only a few times the wavelength of the light. The corresponding power density in these filaments is very high, which makes the Rayleigh, Raman and Brillouin gains very large and results in many shifts. Also self-steepening can be expected at high powers to contribute to the frequency smearing. This smearing has been reported previously by Bloembergen and co-workers,[42] and in CS_2 by Townes and his colleagues.[43]

Usually, the stimulated Raman spectrum is predominant while a small fraction of the total power is spread throughout the rest of the spectrum. When chloronaphthalene or nitrobenzene is used in the cell, the resulting tunable source output power is highest for shifts from the SHG line corresponding to the Raman spectrum. However when CS_2 is used in the liquid cell, almost no structure is observed in the tunable source output power for shifts from the SHG line in excess

of two times the normal CS_2 Raman shifts. Here the laser power output is approximately 30 MW but the power density is 300 MW/cm^2 in the hot spots, and the liquid cell is 32 cm.

The extent of the tunability and the power output of the tunable source is strongly dependent on the incident laser power when one is working near the extremes of the range. Apparently the light not trapped in the small scale filaments after traveling the length of the cell is predominantly input laser light in the long cell limit, while the trapped light is extensively frequency smeared. Attempts to measure the liquid cell output spectrum directly when excited with the Nd laser are now being made.

The reason two additional lines appear when KDP is rotated off the SHG phase matching angle is that there are of course two separate conditions which lead to phase matching for the case of one ordinary ray plus one extraordinary ray producing an extraordinary ray. A plot of the theoretical curves of the phase-matched output frequency versus the internal angle within the KDP measured with respect to the c axis is shown in Fig. IV-6. The experimental points from three different runs are also shown.

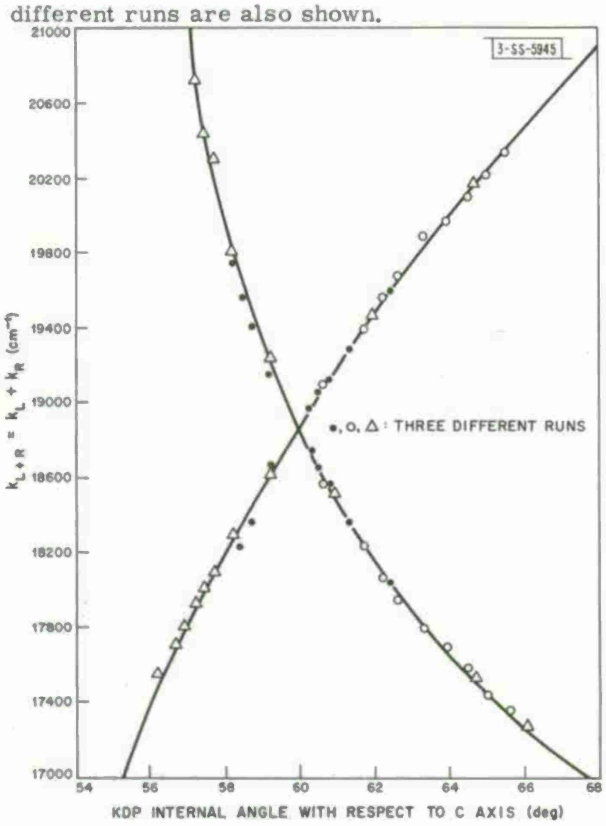

Fig. IV-6. Comparison of theoretical phase matching conditions with experimental data.

This technique can be used to generate tunable sources in the ultraviolet or far-infrared. By using either a ruby or SHG Nd laser as the exciting source, a variable frequency ultraviolet source can be made; by using difference frequency generation techniques, similar for example to those of Martin and Thomas,[44] a tunable far-infrared source should be achievable.

R. L. Carman

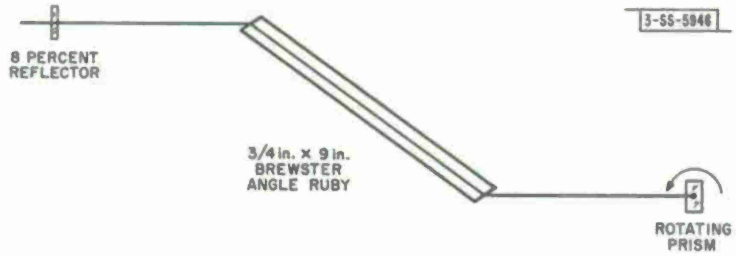

Fig. IV-7. Laser cavity configuration used to observe mode coupling.

5. The Observation of Mode Locking in a Rotating Prism Q-Switched Ruby Laser*

During a series of unrelated experiments, mode locking was observed in the configuration illustrated in Fig. IV-7. The optical cavity length was 73.5 cm, corresponding to a Fabry-Perot $\Delta\nu = c/2L = 240$ MHz or $\tau \equiv \Delta\nu^{-1} = 4.9$ nsec. The output mirror was a resonant reflector with a reflectivity of 8 percent. The number of modes involved was small and the peak power was 50 MW as deduced from an oscillogram (Fig. IV-8) taken with an Optics Technology planar diode

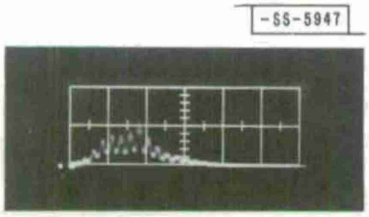

Fig. IV-8. Oscillogram illustrating mode locking (50 MW/cm and 20 nsec/cm). This data was taken with a Tektronix oscilloscope, type 519, and a fast rise diode detector.

detector and a Tektronix 519 scope. The risetime of this system is about 0.6 nsec. This type of output was observed about 20 percent of the time, when the laser was fired near threshold. The relative pulse heights and structure within a pulse varied from observation to observation, as did the net dc average, while the pulse separation remained constant. These results indicate that mode locking of high power lasers is possible without the modulators now used.[45-47]

There are two possible explanations of this effect. First, the ruby rod is not optically pumped over its entire length, so that the unpumped regions may act as a saturable absorber. Because of the rod holders, only 8 of the 9 inches (center to center) of the ruby is excited; and since the whole rod is water cooled, the unpumped ends of the rod can act as a resonant absorber until the population of the excited states equals that of the ground state. For this condition, neither gain nor loss is exhibited in the unpumped regions. The fact that the rod is water cooled may assure that the temperature dependence of the energy difference does not reduce the absorption cross section. While this type of absorber has to "bleach" once, a large mode correlation may be required to achieve the "bleaching" and then stability requirements may cause new modes which are forming to be suppressed. The very narrow pulse widths observed by DeMaria[45] would probably not be achievable this way since no large cross coupling to all modes under the laser gain profile is present, as in the case of a dye type of saturable absorber with a very fast relaxation time. However, this self absorption is capable of acting as a Q-switch in the case of triply-activated glass as shown by Gandy, Ginther, and Weller.[48]

* This research was carried out using the facilities of the National Aeronautics and Space Administration's Electronics Research Center.

Secondly, mode locking may arise from a spatially nonlinear population depletion during the laser action such as was recently discussed by Statz, de Mars and Tang.[49] The sections of the rod in which a lasing Fabry-Perot eigensolution has a node will have a higher population inversion than the anti-node points. Consequently succeeding modes will grow which deplete these more highly populated areas so as to maximize the total emission from the rod. This implies a definite phase relation will exist between all modes that lase. Statz, de Mars and Tang also predict that the pulse spacing for ruby is $\tau = 2L/c$ if the rod is not centered and $\tau = L/c$ if the rod is centered within the optical cavity. In the case of the work reported here, the spacing between the front reflector and the front rod face was optically 15.3 cm while the optical distance between the rotating prism apex and the rear face of the rod was 17.8 cm so that the latter condition is probably applicable and is the one observed.

Statz, de Mars, and Tang[49] have carried out experiments to verify their ideas; for a ruby rod of very short length placed in a long cavity with high reflectivity mirrors on both ends, they have observed outputs which display some mode locking characteristics. However, since their work involves more of a steady state type of situation, it is not necessarily applicable here. In any case, it is believed that this work represents the first reported observation of high power mode locked outputs without the use of separate cavity modulators.

R. L. Carman

6. Far-Infrared Cyanide Laser

We have constructed a cyanide laser which operates at a wavelength of 337 microns.* This radiation source will be used for spectroscopic investigation of solids in the far-infrared. The electric discharge is obtained with a 3000-V, 1-A dc power supply. The distance between reflectors, which are mounted internal to the glass tube, is approximately 220 cm. Output is obtained through a hole in one of the reflectors which is covered with a sapphire window. With only methyl cyanide (CH_3CN) as the flowing vapor, the output power at 337 μ was about 0.2 mW, as measured by means of a Golay cell. The latter was calibrated against a 2 mm carcinotron, whose power output in turn was measured by means of a millimeter wave water-load calorimeter.

C. D. Parker
P. E. Tannenwald

* We wish to acknowledge valuable aid in the construction of the laser provided by Professor Ali Javan and his group at the M.I.T. Physics Department.

REFERENCES

1. E.J. Johnson, Bull. Am. Phys. Soc. 12, 297 (1967).
2. R.J. Elliott and R. Loudon, J. Phys. Chem. Solids 15, 196 (1960).
3. R.L. Bell and K.T. Rogers, Phys. Rev. 152, 746 (1966).
4. R.N. Brown, J.G. Mavroides and B. Lax, Phys. Rev. 129, 2205 (1963).
5. W.J. Scouler, Phys. Rev. Letters 18, 445 (1967).
6. H. Ehrenreich and H.R. Philipp, Phys. Rev. 128, 1622 (1962); B.R. Cooper, H. Ehrenreich and H.R. Philipp, Phys. Rev. 138, A496 (1965).
7. I.M. Templeton, Proc. Roy. Soc. (London) A292, 413 (1966); R. Zallen, Proceedings of the International Colloquium on Optical Properties and Electronic Structure of Metals and Alloys, Paris, 1965 (North-Holland Publishing Company, Amsterdam, 1966), p. 164.
8. M. Garfinkel, J.J. Tiemann, and W.E. Engeler, Phys. Rev. 148, 695 (1966).
9. J.C. Phillips, Phys. Rev. 153, 669 (1967).
10. J. Feinleib, W.J. Scouler and J. Hanus, Bull. Am. Phys. Soc. 12, 347 (1967).
11. R. Bowers and Y. Yafet, Phys. Rev. 115, 1165 (1959).
12. R. Kaplan, Proceedings of the International Conference on Physics of Semiconductors, Kyoto, 1966, J. Phys. Soc. Japan 21 Supplement, 249 (1966).
13. B.G. Dick and A.W. Overhauser, Phys. Rev. 112, 90 (1958).
14. W. Cochran, Proc. Roy. Soc. (London) A253, 260 (1959).
15. G. Dolling, Inelastic Scattering of Neutrons in Solids and Liquids (International Atomic Energy Agency, Vienna, 1964), p. 37.
16. Solid State Research Report, M.I.T. Lincoln Laboratory (1966:3), p. 18, DDC 641498.
17. J.M. Honig, L.L. Van Zandt, J.B. Sohn and T.B. Reed, Bull. Am. Phys. Soc. 12, 399 (1967).
18. D. Adler, Phys. Rev. Letters 17, 139 (1966).
19. A.M. DeGraff and R. Luzzi, Phys. Letters 18, 235 (1965); Phys. Letters 19, 92 (1965).
20. R.E. Newnham and Y.M. De Haan, Zeit. für Kryst. 117, 235 (1962).
21. S.C. Abrahams, Phys. Rev. 130, 2230 (1963).
22. O. Betbeder-Matibet and P. Nozieres, Ann. Phys. 37, 17 (1966).
23. J.M. Luttinger and J.C. Ward, Phys. Rev. 118, 1417 (1960).
24. Solid State Research Report, Lincoln Laboratory, M.I.T. (1966:2) p. 43, DDC 639064.
25. N. Menyuk, K. Dwight, R.J. Arnott and A. Wold, J. Appl. Phys. 37, 1387 (1966), DDC 642203.
26. J.W. Cable, N.K. Wilkinson, E.O. Wollan and W.C. Koehler, Phys. Rev. 125, 1860 (1962).
27. B.R. Cooper, R.J. Elliott, S.J. Nettel and H. Suhl, Phys. Rev. 127, 57 (1962).
28. H.E. Stanley, Phys. Rev. 158, 332 (1967).
29. H.E. Stanley, Phys. Rev. 158, 323 (1967).
30. H.E. Stanley and T.A. Kaplan, Phys. Rev. Letters 16, 981 (1966), DDC 642220.
31. Ref. 29, Appendix I.
32. C. Domb, Adv. Physics 9, 330 (1960), Appendix III.
33. T. Oguchi, J. Phys. Soc. Japan 6, 31 (1951).
34. M.E. Fisher, Am. J. Phys. 32, 343 (1964).

35. H.A. Bethe, Proc. Roy. Soc. (London) A150, 552 (1935); R. Peierls, Proc. Roy. Soc. (London) A154, 207 (1936).

36. H.A. Brown, J. Phys. Chem. Solids 26, 1369 (1965).

37. M.F. Sykes, J. Math. Phys. 2, 52 (1961).

38. G.B. Wright and A. Mooradian, Phys. Rev. Letters 18, 608 (1967).

39. M.M. Litvak, A.L. McWhorter, M.L. Meeks and H.J. Zeiger, Phys. Rev. Letters 17, 821 (1966), DDC 648050; URSI Meeting, Washington, D.C., April 1966; to be published in Astron. J.

40. W.M. Goss, "OH Absorption in the Galaxy," Ph.D. Thesis, Berkeley Radio Astronomy Laboratory, University of California (1967).

41. C.V. Heer, Phys. Rev. Letters 17, 774 (1966) and to be published in Phys. Letters; P.L. Bender, Phys. Rev. Letters 18, 562 (1967).

42. N. Bloembergen and P. Lallemand, Phys. Rev. Letters 16, 81 (1966).

43. C.H. Townes and co-workers, private communication.

44. M.O. Martin and E.L. Thomas, IEEE J. Quant. Elec. QE-2, 196 (1966).

45. A.J. DeMaria, D.A. Stetser and H. Heynau, Appl. Phys. Letters 8, 174 (1966); A.J. DeMaria, C.M. Ferrar and G.E. Davidson, Jr., Appl. Phys. Letters 8, 22 (1966).

46. H.W. Mocker and R.J. Collins, Appl. Phys. Letters 7, 270 (1965).

47. T. Deutsch, Appl. Phys. Letters 7, 80 (1965).

48. H.W. Gandy, R.J. Ginther and J.F. Weller, Appl. Phys. Letters 7, 233 (1965).

49. H. Statz, G. De Mars and C.L. Tang, to be published; C.L. Tang and H. Statz, J. Appl. Phys. 38, 323 (1967); C.L. Tang and H. Statz, Phys. Rev. 128, 1013 (1962).

UNCLASSIFIED
Security Classification

DOCUMENT CONTROL DATA – R&D

(Security classification of title, body of abstract and indexing annotation must be entered when the overall report is classified)

1. ORIGINATING ACTIVITY *(Corporate author)* Lincoln Laboratory, M.I.T.	2a. REPORT SECURITY CLASSIFICATION Unclassified 2b. GROUP None
3. REPORT TITLE Solid State Research	
4. DESCRIPTIVE NOTES *(Type of report and inclusive dates)* Quarterly Technical Summary – 1 February through 30 April 1967	
5. AUTHOR(S) *(Last name, first name, initial)* McWhorter, Alan L.	
6. REPORT DATE 15 May 1967	7a. TOTAL NO. OF PAGES 72 / 7b. NO. OF REFS 95
8a. CONTRACT OR GRANT NO. AF 19 (628)-5167 b. PROJECT NO. 649L c. d.	9a. ORIGINATOR'S REPORT NUMBER(S) Solid State Research (1967:2) 9b. OTHER REPORT NO(S) *(Any other numbers that may be assigned this report)* ESD-TR-67-266
10. AVAILABILITY/LIMITATION NOTICES Distribution of this document is unlimited.	
11. SUPPLEMENTARY NOTES None	12. SPONSORING MILITARY ACTIVITY Air Force Systems Command, USAF

13. ABSTRACT

This report covers in detail the solid state research work at Lincoln Laboratory for the period 1 February through 30 April 1967. The topics covered are Solid State Device Research, Optical Techniques and Devices, Materials Research, and Physics of Solids.

14. KEY WORDS

solid state devices	band structure	Fourier expansion	crystal growth
electron beam pumping	Raman scattering	phonons	electroluminescence
optical techniques and devices	magnetoabsorption	magnetism	magneto-optical research
laser research	vapor growth	Faraday isolator	infrared
materials research	magnetoreflection	heterodyne detection	

UNCLASSIFIED
Security Classification

Printed by
United States Air Force
L. G. Hanscom Field
Bedford, Massachusetts